PHILOSOPHICAL TRANSACTIONS OF THE ROYAL SOCIETY A MATHEMATICAL, PHYSICAL & ENGINEERING SCIENCES

Experiments with Plasma Waves

J. O. Thomas

Phil. Trans. R. Soc. Lond. A 1975 **280**, 193-224
doi: 10.1098/rsta.1975.0100

Phil. Trans. R. Soc. Lond. A. **280**, 193–224 (1975) [193]
Printed in Great Britain

Experiments with plasma waves

By J. O. Thomas
Physics Department, Imperial College, University of London

[Plate 11]

Plasma waves play an important role in planetary plasma envelopes and in astrophysical plasmas. They occur naturally, for example, in the Earth's ionosphere and magnetosphere where they have been detected by rockets and satellites. Historically, the kinds of modes predicted increased both in number and in diversity as cold plasma theory was extended to include the effects of external magnetic fields and of finite plasma temperatures.

Attention is mainly concentrated in the paper on waves propagating in a narrow band of frequencies near the plasma frequency, f_N, and on those often referred to as the electron Bernstein modes. The latter propagate with wavevectors in a direction closely perpendicular to an applied magnetic field. Their existence is not predicted by cold plasma theory. They are, however, easy to excite in relatively simple laboratory experiments and provide an instructive laboratory demonstration of effects depending on thermal motions in a plasma. An interference experiment designed to detect and to make measurements on such waves is described. Dispersion properties are in good agreement with the predictions of the kinetic theory of hot magnetoplasmas.

Three dimensional ray tracing in hot magnetoplasmas in a narrow band of frequencies near the plasma frequency, including Doppler shifts, has confirmed the feasibility of a plasma wave radar which can provide a good technique for determining electron temperatures and densities and their gradients. Computational and analytical techniques have been proposed to determine these quantities.

The paper concludes with a brief assessment of the use of plasma waves in space and laboratory plasma diagnostics.

1. Introduction

Plasma waves play an important role not only in laboratory experiments involving plasmas but in the physics of planetary ionospheres and magnetospheres, in the aurora, in the Sun and in other astrophysical plasmas. At this Royal Society Discussion Meeting on the theory of electric and magnetic waves in the ionosphere and in the magnetosphere, it is appropriate that the main emphasis in my paper should be directed towards those experiments with plasma waves which are rather directly related to, and indeed arise from, my interest in the interpretation and understanding of data recorded by satellites and rockets launched to investigate the properties of the Earth's plasma envelope (such data often contain signals associated with what have become known as plasma 'resonance' effects and I shall return to these in a later section). Thus I shall make no attempt to review, even briefly, the extensive theoretical and experimental work extant in the scientific literature on plasma waves, instead the reader is referred to the first of the two volumes entitled *Plasma waves in space and laboratory* published by the Edinburgh University Press (Thomas & Landmark 1969, 1970) which contains a number of review papers. The second volume is devoted to accounts of recent researches in the subject by individual scientists. Perhaps I should also mention the recent new book *Plasma physics* edited by Keen (1974) which contains a number of review papers directly related to our field. In this paper, I shall describe work carried out

recently in the Physics Department at the Imperial College of Science and Technology in the University of London and sponsored by the Science Research Council.

The subject with which I am going to deal concerns the application of simple wave theory to describe the linear responses of the plasma at, or very near to, the plasma 'characteristic' frequencies ω_p, ω_T and $n\omega_H$ listed in table 1 in which the preferred nomenclature of ionospheric physicists, as distinct from their laboratory counterparts, has been given priority. The responses take the form of propagating waves of different kinds, but in what follows, I shall restrict myself to describing experiments on waves which are not predicted by cold plasma theory, i.e. they cannot be accounted for by standard Appleton–Hartree magnetoionic theory in which the plasma temperature is taken to be zero and which is normally adequate to describe the propagation of radio waves in the ionosphere, at any rate from the point of view of radio communication. It should be noted, parenthetically, that signals referred to in the literature as 'resonances', 'diffuse resonances', 'remote resonances' or 'plasma spikes' occur at a number of frequencies not included in table 1 and that beat notes between fundamental frequencies and between overtones as well as the transfer of energy from one resonance frequency to another have been reported. Non-linear wave-particle interactions involving coupling between three waves under weak turbulence caused by local plasma temperature anisotropies have been evoked to explain some of the observations. Neither such observations themselves, nor the theoretical explanations offered, will be discussed in this paper: useful references to such observations and to the theory of non-linear effects in plasmas are given by Thomas & Andrews (1969) and by Franklin (1974), and Cook (1974) respectively. The review by Wesson (1974) contains references to the extensive literature on plasma instabilities – another related and topical subject not treated in the present work. To conclude this introduction, it should be mentioned that plasma inhomogeneities and the existence of plasma boundaries, common in laboratory plasma experiments, may be of less importance in space experiments involving plasma waves. The mathematical complexity of theoretical work in the fields described above is such that attempts to derive numerical solutions still often tax the capacity of the largest and fastest computers. For example, the analyses normally deal with infinitesimally small antennae immersed (usually) in a collisionless, homogeneous, plasma of infinite extent. A great deal remains to be done on the physics of ion sheaths surrounding antennae immersed in plasmas and relatively little is known on the detailed mechanism of how plasma waves are excited and coupled to the plasma itself – a problem which has been discussed recently (Derfler 1974) in connexion with radio frequency plasma heating to produce thermonuclear fusion energy.

We now describe some experiments with plasma waves and present the relevant theoretical background briefly. Following this, recent developments in ray tracing in hot magnetoplasmas leading to the concept of plasma wave radars involving stationary or moving sources will be presented. The problems involved in recording plasma wave ionograms will be mentioned together with possible solutions. The advantages of using plasma waves for space and laboratory plasma diagnostics are then evaluated briefly and possible applications in some physics experiments outlined.

2. General theoretical background

The basic idea that electrons, initially displaced in a cold plasma, will oscillate under the influence of the restoring force (due to charge separation) exerted upon them by the more massive and therefore relatively stationary ions is well known and leads to a simple harmonic vibration of

the electrons at the plasma angular frequency, ω_p (table 1). The presence of a static magnetic field, of course, modifies the frequency at which the oscillation takes place. Landau (1946) showed that the simple oscillation at the plasma frequency could and would be changed into slowly propagating, damped, waves. Landau's contribution was to include the effect of thermal motions of the electrons arising from a finite plasma temperature. Bernstein (1958) and others developed the analysis of Landau to include the effects of a static magnetic field superimposed on the plasma and this extension led to the prediction of wave propagation modes at frequencies equal to multiples of the electron gyrofrequency.

These have become known as the electron gyroresonance, electron cyclotron, or, Bernstein modes. Corresponding modes related to the ion gyrofrequency are now also known (Fredricks 1968). Those wave modes in which the ions play the dominant role and low frequency waves near the ion cyclotron, ion plasma or lower hybrid frequencies, are not discussed in this paper.

TABLE 1. MAGNETOIONIC CONDITIONS AND PLASMA CHARACTERISTIC FREQUENCIES AT WHICH THE MAIN SPIKE-LIKE RESPONSES MAY BE SEEN ON TOPSIDE SOUNDER RECORDS: 'RESONANCE' PHENOMENA ALSO SOMETIMES OCCUR AT FREQUENCIES NOT LISTED IN THE TABLE (SEE TEXT)

$X = \omega_p^2/\omega^2$, $Y = \omega_H/\omega$ (see table 2)

magnetoionic condition	remark	frequency
$X = 1$	plasma 'resonance' or 'spike'	$\omega^2 = \omega_p^2$
$X = 1 - Y^2$	upper hybrid resonance	$\omega_T^2 = \omega_p^2 + \omega_H^2$
$Y = 1/n$	gyroresonances and harmonics: $n = 1, 2, 3, \ldots$	$\omega = n\omega_H$

In a real, hot, magnetoplasma, it is thus important to include the effects of thermal motions which cause the particles to gyrate about the ambient magnetic field direction with finite cyclotron radii. In the presence of an alternating electric field (e.g. the r.f. field produced by a driven satellite antenna), the electrons become bunched spatially within their orbits (Lockwood 1963). The electrons will continue to travel in bunches after the applied field is removed and will generate an electromagnetic field oscillating at the electron cyclotron frequency. A similar model, incorporating a gradient of the electric field of the transmitter near the satellite, accounts for a gain of energy by the electrons at harmonics of the cyclotron frequency. In practice, the particles involved will have many different velocities, some of them matching the speed of a wave propagating through the medium and strong wave-particle resonant interactions can then result. These interactions and the collective effects of the particles were included in the treatment of the problem by Landau through the introduction of a velocity distribution function, leading, as stated earlier, not only to a description of propagating waves at the plasma frequency, but, also, the prediction of new modes at other frequencies when a static magnetic field was included.

3. THEORY OF PROPAGATION OF PLASMA WAVES

The basic theory of propagation of plasma waves in infinite plasmas has been extensively treated elsewhere and the reader is referred to the books and other references numbered [1]–[12] in the paper by Crawford (1969) and to reviews by Dougherty (1974) and Sanderson (1974) and to the references quoted therein. Appendix A contains some of the main points in the relevant general theory including a discussion of the plasma permittivity and the dispersion relation

PHILOSOPHICAL TRANSACTIONS OF THE ROYAL SOCIETY A MATHEMATICAL, PHYSICAL & ENGINEERING SCIENCES

satisfied by the relevant plasma wave modes. It includes a discussion of the electron oscillations in a hot plasma. The nomenclature is that shown in tables 1 and 2.

I have hitherto refrained from using the term 'electrostatic' waves. This adjective, often used in the literature to describe these waves, refers essentially to the 'electrostatic approximation' in the mathematical analysis. It is assumed that there is no magnetic field for the wave itself, in other words, the wavevector, $\boldsymbol{k}$, is sufficiently parallel to the wave electric field, $\boldsymbol{E}$, that the induced magnetic field, given by Maxwell's third equation (A 1) is negligibly small. Thus $\boldsymbol{E}$ is derivable from a scalar potential, ϕ, as in electrostatics, i.e Poisson's equation for the plasma is

$$\nabla \cdot \boldsymbol{\varepsilon} \cdot \nabla \phi = 0,$$

and the wave equation (appendix A) may be written

$$\boldsymbol{k} \cdot \boldsymbol{\varepsilon} \cdot \boldsymbol{k} = 0$$

in which $\boldsymbol{\varepsilon}$ is the permittivity tensor.

TABLE 2. NOMENCLATURE

a	Debye length $= (\epsilon_0 KT/Ne^2)^{\frac{1}{2}}$	t	time
$\boldsymbol{B}, \boldsymbol{B}_0$	magnetic induction $= \mu_0 \boldsymbol{H}$	T	absolute electron temperature
c	speed of light *in vacuo*	$\boldsymbol{v}$	particle velocity
$\boldsymbol{D}$	electric displacement	$\boldsymbol{v}_g$	group velocity
e	electronic charge (positive) (also used for the exponential function)	v_T	thermal speed of an electron, $\sqrt{\left(\frac{KT}{m}\right)}$
$\boldsymbol{E}, \boldsymbol{E}_0$	electric field	X	$f_N^2/f^2 = \omega_p^2/\omega^2$.
f, f_0	wave frequency	Y	$f_H/f = \omega_H/\omega$. Also used for admittance, $1/Z = G + \mathrm{i}S$
f_H	electron gyrofrequency, $\omega_H/2\pi$	Z	impedance
f_N	plasma frequency	$\boldsymbol{\varepsilon}$	tensor permittivity
f_T	upper hybrid frequency	$\epsilon_\perp$	perpendicular component of $\boldsymbol{\varepsilon}$; $\epsilon_\perp(k, \omega) \equiv \epsilon(k_\perp, \omega)$
G	conductance	ϵ_0	permittivity of free space
$\boldsymbol{H}$	magnetic field (unless otherwise stated)	λ	wavelength, $2\pi/k$
i	$\sqrt{-1}$	Λ	$k_\perp^2 r^2$
$\boldsymbol{k}$	wavevector, components k_x, k_y, k_z. Note that k is often written for $\lvert\boldsymbol{k}\rvert$.	μ_0	permeability of free space
$k_\perp$	propagation vector in direction perpendicular to $\boldsymbol{B}_0$†	ν	collision frequency between electrons and neutral particles
K	Boltzmann constant	ϕ	phase angle (unless otherwise stated)
m	electron mass	ω, ω_0	$2\pi f$ or $2\pi f_0$
n	an integer, 1, 2, 3, ...	ω_H	electron angular gyrofrequency, $\lvert e\boldsymbol{B}_0/m\rvert$
N	electron density	ω_p	plasma frequency $2\pi f_N$
r	the electron gyroradius $\frac{1}{\omega_H}\sqrt{\left(\frac{KT}{m}\right)}$	ω_T	$2\pi f_T$
$\boldsymbol{r}$	position vector	Ω	dispersion parameter f/f_H
S	susceptance		

† Where it is clear that propagation perpendicular to $\boldsymbol{B}_0$ is involved throughout, the suffix $\perp$ may be dropped.

The components of the electric field $\boldsymbol{E}$ parallel and perpendicular to $\boldsymbol{k}$ may be incorporated into the *full* wave equation ((1–17) of Stix 1962) to give

$$(\epsilon_0 n^2 - \boldsymbol{\varepsilon}\cdot)\,\boldsymbol{E}_\perp = \boldsymbol{\varepsilon}\cdot\boldsymbol{E}_\parallel, \tag{1}$$

where ϵ_0 is the permittivity of free space and n is the refractive index, ck/ω, of the plasma. Since $\boldsymbol{E}_\perp \to 0$ and the waves are purely longitudinal, it follows from the wave equation above that n is large i.e. ck/ω is large or ω/k, the phase velocity of the wave $\ll c$. Thus the value of $k = \lvert\boldsymbol{k}\rvert$ must not become too small and we are dealing with short wavelength, slow waves.

The nature of the tensor permittivity to be inserted in equation (A 8) depends on the analysis of the particular equations of motion for the particles. For example, if the Lorentz force is used in the equation of motion to describe the effect of an electric and magnetic field on the moving particles, then cold plasma theory predicts a number of waves including those known as the ordinary and extraordinary rays in ionospheric terminology. New modes are predicted when plasma thermal motions are allowed for. The particle motions are now accounted for by the Boltzmann equation and a particle velocity function $f(\boldsymbol{r}, \boldsymbol{v}, t)$.

The external charge, ρ_{ext}, on an antenna immersed in a plasma is related to the Laplace and Fourier transformed electric field by the general equation (A 11) derived in appendix A which may be written in the form

$$\boldsymbol{E}(\boldsymbol{k}, \omega) = \mathrm{i}\boldsymbol{k}\rho_{\text{ext}}/\boldsymbol{k}.\boldsymbol{\varepsilon}(\boldsymbol{k}, \omega).\boldsymbol{k}.$$

For propagation perpendicular to the applied magnetic field, $\boldsymbol{B}_0$, (A 11) quoted above becomes (A 14) which may be written†

$$\epsilon_\perp(k, \omega)\, \boldsymbol{E}(\boldsymbol{k}, \omega) = \mathrm{i}\boldsymbol{k}\rho_{\text{ext}}/k^2. \tag{2}$$

Since for propagating plasma waves we require non-zero values of E to exist in the absence of ρ_{ext}, it follows from (2) that

$$\epsilon_\perp(k, \omega) = 0$$

where $\epsilon_\perp$ is the component of the permittivity tensor perpendicular to $\boldsymbol{B}_0$.

By allowing for the thermal motion of the electrons in the way mentioned above, Bernstein (1958) derived a dispersion relation for electron oscillations in a warm plasma and showed that the modes with $\boldsymbol{k}$ perpendicular to $\boldsymbol{B}_0$ were not subject to Landau damping. The dispersion equation, given as (A 17) may be written

$$\frac{\epsilon_\perp(k, \omega)}{\epsilon_0} = 1 - \frac{\omega_p^2}{\omega_H^2} \sum_{n=1}^{\infty} \frac{2\exp(-\Lambda)\, I_n(\Lambda)}{\Lambda((\omega/n\omega_H)^2 - 1)} = 0, \tag{3}$$

where $\Lambda = (k_\perp^2/\omega_H^2)\,(KT/m) = (k_\perp r)^2$ and r is the gyroradius of an electron with thermal energy. I_n is a Bessel function of imaginary argument. The other symbols are as defined in table 2. The derivation of (3) is described briefly in appendix A.

The lines shown in figure 1 represent schematically the two basic forms which the dispersion curves take under certain circumstances – some numerical solutions are given in figure 2. A frequency ω_0 lying in a pass band and applied to an antenna in a plasma (figure 1) would excite either one mode ($\omega_0 < \omega_T$) or the two wavenumbers $\pm k_1$ and $\pm k_2 (\omega_0 > \omega_T)$. It should be noted that positive group velocities correspond to $-k_1$ (the high k mode – i.e. the short wavelength mode) and to $+k_2$ (the low k mode or long wavelength mode). This is obvious from figure 1 since the group velocity is simply the slope, $\mathrm{d}\omega/\mathrm{d}k_\perp$, of the dispersion curve. Thus, though one mode has a negative phase velocity, the energy is always carried away (group velocity positive) from the antenna (see appendix A).

The form of f/f_H as a function of $k_\perp r$ is shown in figure 2 as a series of propagation pass bands.

The plasma admittance (which is amenable to experimental measurement) may be derived by

† In (2) and subsequent equations concerned with Bernstein modes, it is to be understood that the wavevector, $\boldsymbol{k}$, is that for the modes perpendicular to $\boldsymbol{B}_0$, i.e. the k_x or $k_\perp$ modes. The suffix $\perp$ is retained only where necessary for emphasis. Thus the relevant component of $\boldsymbol{\varepsilon}(\boldsymbol{k}, \omega)$ to be substituted in the general equation (A 11) is $\epsilon_\perp = \epsilon_{xx}$ (Stix 1962) and in our nomenclature $\epsilon_\perp(k, \omega)$ is equivalent to $\epsilon(k_\perp, \omega)$. Since propagation is now restricted to be perpendicular to $\boldsymbol{B}_0$ in the positive x-direction, we subsequently write the vector electric field as $E(x, \omega)$, $E(x, t)$, etc.

considering the electric field in the plasma as a function of space and frequency. Performing the inverse Fourier transform, equation (2) becomes

$$E(x,\omega) = \frac{1}{2\pi}\int_{-\infty}^{+\infty} \frac{\mathrm{i}\rho_{\mathrm{ext}}\,\mathrm{e}^{-\mathrm{i}kx}}{k\epsilon_{\perp}(k,\omega)}\,\mathrm{d}k. \tag{4}$$

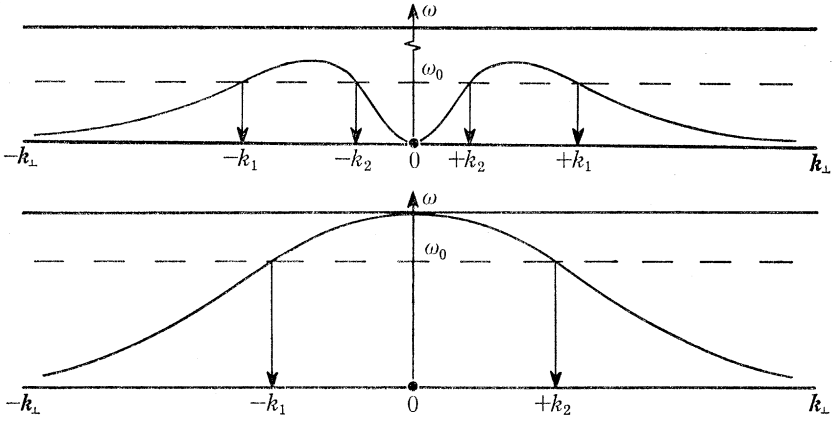

FIGURE 1. Schematic diagram to represent the forms the dispersion relations for the Bernstein modes may take when $\omega_0 > \omega_H$ and when $\omega_0 < \omega_H$ (upper and lower curves respectively). $\epsilon(k_\perp, \omega_0)$ is zero at $\pm k_1$ and $\pm k_2$ (upper curve) and the modes excited with positive group velocities are $-k_1$ and $+k_2$. For $\omega_0 < \omega_H$ only one mode is excited when a signal of frequency ω_0 is applied. The origins for the $k_\perp$ axes (only) are marked. The horizontal thick lines occur at consecutive integral multiples of ω_H.

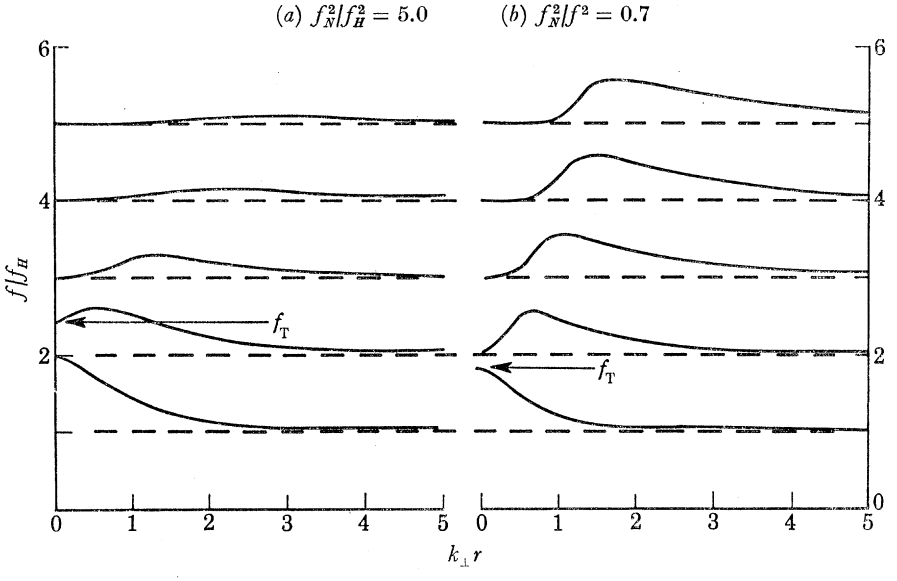

FIGURE 2. Some typical numerical solutions of equation (3), $\epsilon(k_\perp, \omega) = 0$. These represent the dispersion relation $(k_\perp, \omega)$ for cyclotron waves propagating at right angles to $\boldsymbol{B}_0$. The curves have been normalized by plotting f/f_H and $k_\perp r$ where r is the gyroradius of an electron with thermal energy and so depends on the electron temperature. In curves (*a*) the ratio f_N^2/f_H^2 is constant and in curves (*b*) the ratio f_N^2/f^2 is constant. In each case, propagation above f_T, the upper hybrid frequency is possible only in pass bands just above the gyroharmonics. Only values for positive $k_\perp r$ are plotted: the curves have mirror images about the ordinate axis through $k_\perp r = 0$ (from Andrews 1969).

4. Antennae immersed in plasmas

In practice, it may be assumed that ρ_{ext} is applied as a radio frequency voltage on an antenna immersed in the plasma in the (y, z) plane, parallel to $\boldsymbol{B}_0$, and hence produces only an x component of the electric field. The character of the electric field is seen from (4) to be determined by the poles in the integrand produced by the roots of the dispersion equation $\epsilon_\perp(k, \omega) = 0$ in the denominator and by the presence of the exponential term which will introduce oscillations in the electric field corresponding to one or two wavenumber modes. In the absence of collisions, when the frequency lies within a pass band, real roots of $\epsilon(k_\perp, \omega)$ lie on the real $k_\perp$ axis. In the presence of collisions, the roots of $\epsilon(k_\perp, \omega)$ become complex and the integration can be performed entirely along the real $k_\perp$ axis.

In the presence of collisions we may write, for large t; putting $\omega = \omega_0$,

$$\boldsymbol{E}(x, t) = \frac{\mathrm{e}^{\mathrm{i}\omega_0 t}}{2\pi} \int_{-\infty}^{+\infty} \frac{\mathrm{i}\boldsymbol{k}\, \mathrm{e}^{-\mathrm{i}kx}\, \mathrm{d}k}{k^2 \epsilon_\perp(\omega_0 - \mathrm{i}\nu, k)}. \tag{5}$$

Two types of antenna structure have been treated in some detail, namely, parallel cylindrical conductors (wires) and infinite parallel grids by Mantei (1967), and the latter by Buckley (1968; 1970). The relevant theory is summarized briefly in appendix B. Basically it consists in substituting for ρ_{ext} into equation (4) and integrating to obtain the field. The current is obtained as the time derivative of ρ_{ext}. If a sinusoidal voltage of frequency ω is applied to the antenna and $q(t)$ is the resulting charge per unit area, then the current is

$$I_0 = \mathrm{i}\omega q. \tag{6}$$

The plasma admittance per unit area for an antenna separation d is then given by

$$Y(\omega) = \frac{\mathrm{i}\omega q}{\int_0^d E(x, \omega)\, \mathrm{d}x}. \tag{7}$$

In our experiments we have used both parallel wires and parallel grids. Clearly in each case, the admittance, Y, will be governed by the detailed behaviour of $E(x, \omega)$ as given in (4). For the case of two wires, Mantei (1967) has derived the expression (B 3) for the admittance and has computed the conductance G, the susceptance S and the modulus of the plasma admittance given by $|Y| = (G^2 + S^2)^{\frac{1}{2}}$ in the presence of collisions. The results are basically identical with those of the grids though, in practice, the maxima of admittance are relatively accentuated by the comparatively lower vacuum capacitance of the two parallel wires and the experimental results, given later, are for this case. The plasma admittance effects in which we are interested are, however, essentially independent of the detailed antenna geometry (except near the sheaths) and arise from the zeros of $\epsilon(k_\perp, \omega)$ and the exponential term in (4) and (5). The effects will be illustrated below by reference to the parallel grid case for which the mathematical expressions for the electric field and for the plasma admittance are somewhat simpler than for the parallel wire case.

(a) *Parallel infinite grids immersed in a plasma*

For parallel grids Mantei (1967) gives

$$Y(\omega) = \mathrm{i}\pi\omega \Big/ 2 \int_{-\infty}^{\infty} \frac{\sin^2(k_\perp x_0)\, \mathrm{d}k_\perp}{k_\perp^2\, \epsilon(k_\perp, \omega)}, \tag{8}$$

where x_0 is half the grid separation and the integration is carried out with respect to $k_\perp$.

It is clear that the admittance for a fixed grid separation will contain an oscillatory component arising from the $\sin^2(k_\perp x_0)$ term and will also depend on the behaviour of the denominator in the integrand. The detailed behaviour of the latter, which produces the main large effects, is discussed in appendix B but essentially the effect is to increase the admittance near the gyroharmonics. *The effect of the oscillatory component* $\sin^2(k_\perp x_0)$ *is subsidiary and is illustrated in figure* 3. Subsidiary admittance maxima due to this oscillatory component correspond to minima of $\sin(k_\perp x_0)$ in the integration of (8), i.e. to an even number of half wavelengths between grids and the subsidiary admittance minima correspond to maxima of $\sin(k_\perp x_0)$ in the integration i.e. to an odd number, of half wavelengths between grids.

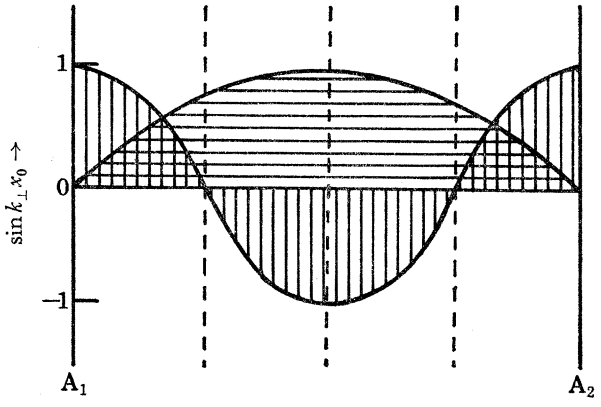

FIGURE 3. A subsidiary *maximum* of the admittance Y, occurs when there is a *minimum* of $\sin^2 k_\perp x_0$ in the integral in (8), i.e. when an even number of half wavelengths is contained between the antennae A_1, A_2 (vertical shading integrates to zero in schematic diagram above). A subsidiary minimum of Y occurs when the integrated area is a maximum, i.e. when an odd number of half wavelengths (horizontal shading) is contained between the antennae.

Buckley (1968, 1970), in an analysis for parallel grids, similar to that of Mantei (1967), has expanded (5) for vanishingly small ν as a sum of residuals corresponding to the poles of the integrand. The result due to one grid, is of the form, for unit charge per unit area,

$$E(x,t) = -\mathrm{e}^{\mathrm{i}\omega_0 t}\left(\frac{1}{2\epsilon_\perp(\omega_0)|_{k=0}} + \frac{\mathrm{e}^{+\mathrm{i}k_1 x}}{-k_1\,\partial\epsilon_\perp/\partial k|_{-k_1}} + \frac{\mathrm{e}^{-\mathrm{i}k_2 x}}{k_2\,\partial\epsilon_\perp/\partial k|_{k_2}} + 2\,\mathrm{Re}\sum_{n=3}^{\infty}\frac{\mathrm{e}^{-\mathrm{i}k_n x}}{k_n\,\partial\epsilon_\perp/\partial k|_{k_n}}\right), \tag{9}$$

in which it should be noted that in general $\partial\epsilon_\perp/\partial k|_{-k_n} = -\partial\epsilon_\perp/\partial k|_{+k_n}$ where $n = 1, 2, 3, \ldots$.

The expression (9) above contains the terms $k\,\partial\epsilon_\perp/\partial k|_k$ in the denominators on the right hand side so that in the passbands near multiples of the electron gyrofrequency there is, as a result, a decrease in Z or an increase in admittance due to the presence of the warm plasma effects. Equation (9) is worthy of consideration in some detail. First we see that the field (and through (7) the impedance) is made up of basically three contributions.

(i) *Effects due to the pole at* $k = 0$ *– the cold plasma contribution*

Suppose $k_1, k_2, k_3, \ldots$, are infinite. The only contribution to the impedance then comes from the term k_0. The denominator of the first term in (9), arising from the pole at $k = 0$ is found by equation (A 17) appendix A to be

$$\epsilon_\perp|_{k=0} = \epsilon_0\left(1 - \frac{\omega_\mathrm{p}^2/\omega_H^2}{\omega_0^2/\omega_H^2 - 1}\right). \tag{10}$$

and is just ϵ_c, the cold plasma perpendicular permittivity. Thus term 1 represents the capacitively transmitted field, with an infinite wavelength in the electrostatic approximation. For $\omega_p = 0$, $\epsilon_c/\epsilon_0 = 1$ corresponding to a pure susceptance of unit magnitude.

(ii) *Effects due to the terms in* $-k_1$ *and* k_2

The terms in (9) involving $-k_1$ and k_2 represent the hot plasma effects (not predicted on simple theory) and correspond to the undamped, Bernstein modes. In the stop-band zones, both k modes are non-existent for purely vertical propagation ($\boldsymbol{k}$ perpendicular to $\boldsymbol{B}_0$). Below ω_T, only one k mode is excited – the $-k_1$ mode. The exponential terms in the numerators in (9) will produce oscillations of $\boldsymbol{E}$ if the antenna separation x is increased.

(iii) *Effects due to the final terms* $k_3, k_4, \ldots$

The final summation in (9) expresses the spatially damped contribution from any complex zeros of $\epsilon_\perp$, which arise, for example, when ω_0 lies outside a propagating cyclotron band. Roots $\pm k$ of $\epsilon_\perp$ then appear in complex conjugate pairs. This summation rapidly decays as x increases. For very small values of x it can be regarded as accounting for the effects of the radio frequency plasma sheath surrounding the probe.

In general, the impedance $Z = 1/Y = R + \mathrm{i}X$ per unit area and is obtained by inverting (7).

(1) *Fixed grid separation* (ω_H/ω *varied*, ω_p *constant*). For a grid separation distance $x = d$, and $\omega = \omega_0$ (7) and (9) yield for the impedance,

$$Z = -\left(\frac{\epsilon_0}{\epsilon_c}\right)\left(\frac{\mathrm{i}}{\omega_0 C_0}\right) + \frac{2}{\omega_0 C_0 d}\left(\frac{1-\mathrm{e}^{+\mathrm{i}k_1 d}}{-k_1^2\,\partial\epsilon_\perp/\partial k|_{-k_1}} - \frac{1-\mathrm{e}^{-\mathrm{i}k_2 d}}{-k_2^2\,\partial\epsilon_\perp/\partial k|_{k_2}}\right), \tag{11}$$

omitting the spatially damped terms with $n \geqslant 3$ which arise from (9) when ω_0 lies outside the Bernstein mode propagation pass bands and assuming $d > a$, the Debye length. In (11) C_0 is the *vacuum* capacitance per unit area. (11) can be split into its real and imaginary parts giving

$$R = \frac{1}{\omega_0 C_0}\frac{2}{d}\left(\frac{1-\cos k_1 d}{-k_1^2\,\partial\epsilon_\perp/\partial k|_{-k_1}} - \frac{1-\cos k_2 d}{k_2^2\,\partial\epsilon_\perp/\partial k|_{k_2}}\right), \tag{12}$$

$$X = -\frac{\epsilon_0}{\epsilon_c}\frac{1}{\omega_0 C_0} + \frac{2}{d\omega_0 C_0}\left(\frac{\sin k_1 d}{k_1^2\,\partial\epsilon_\perp/\partial k|_{-k_1}} - \frac{\sin k_2 d}{k_2^2\,\partial\epsilon_\perp/\partial k|_{k_2}}\right). \tag{13}$$

From (12) we see that since $\partial\epsilon_\perp/\partial k|_{-k_1} < 0$ and $\partial\epsilon_\perp/\partial k|_{k_2} < 0$, then $R \geqslant 0$ as it should be.

These equations again show that in the Bernstein mode pass bands, both the real and imaginary parts of the impedance contain oscillatory terms. Thus as f_H/f is varied in an actual experiment there will (in addition to the superimposed warm plasma effects giving a general increase of admittance in the band pass zones) be subsidiary maxima and minima of the admittance as the $\sin kd$ and/or $\cos kd$ terms go through maxima and minima.

To illustrate what happens, consider the situation when $\omega_0 < \omega_T$ then (12) shows that

$$R = \frac{2}{\mathrm{d}\omega_0 C_0}\left(\frac{1-\cos k_1 d}{-k_1^2\,\partial\epsilon_\perp/\partial k|_{-k_1}}\right), \tag{14}$$

so that the real part of the admittance arises solely from the Bernstein mode and as $d \to \infty$, $\omega_0 C_0 R \to 0$. Writing $C_0 = \epsilon_0/d$ we see that

$$R = \frac{2}{\epsilon_0 \omega_0}\left(\frac{1-\cos k_1 d}{-k_1^2\,\partial\epsilon_\perp/\partial k|_{-k_1}}\right). \tag{15}$$

In addition, as $d \to \infty$, (13) shows that

$$iX \to \frac{1}{i\omega_0 C_0}\left(\frac{\epsilon_0}{\epsilon_c}\right) = \frac{1}{i\omega_0}\frac{d}{\epsilon_c} = \frac{1}{i\omega_0 C}, \tag{16}$$

where C is the *cold plasma* capacitance per unit area, and we see that, in general, the admittance of a plasma can be regarded as being made up of a part proportional to $|\epsilon_c/\epsilon_0|$ with additional superimposed warm plasma contributions. Thus the signal received in an experiment in which a radio frequency is transmitted from one antenna to another in the plasma will be related to $|\epsilon_c/\epsilon_0|$ (figure 4, figure 8).

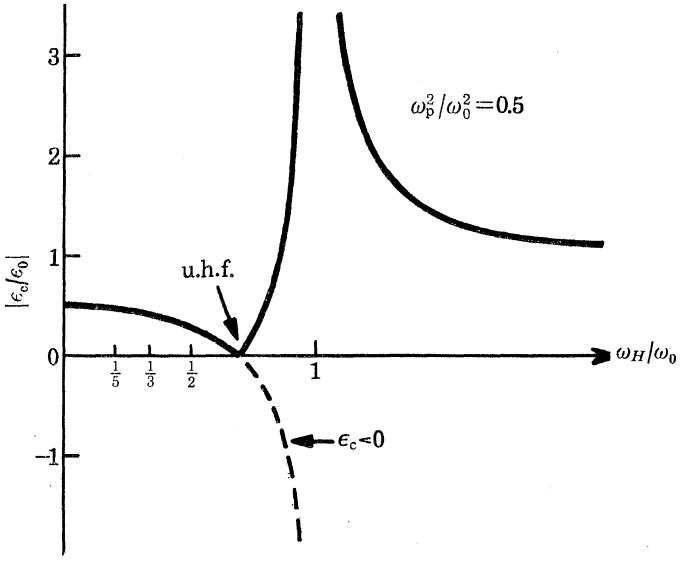

FIGURE 4. The modulus of the scalar cold plasma permittivity, ϵ_c/ϵ_0, (ϵ_0 is the permittivity of free space) as a function of ω_H/ω_0 calculated from (10). The curve also gives the overall shape of the perpendicular admittance between two antennae in a magnetoplasma. Hot plasma effects are superimposed on the cold plasma variations and the curves should be compared with those obtained experimentally, figure 8*a*, *b*, *c*. Note the admittance null at the upper hybrid frequency and the infinity at $\omega_H/\omega_0 = 1$.

In general, in the pass bands close to integral multiples of the electron gyrofrequency, the effects are such that if we write the interelectrode capacitance as

$$C = \epsilon_r C_0,$$

then $Z = 1/i\omega C$ and $Y = i\omega C = i\omega C_0 \epsilon_r(\omega, \omega_H, \omega_p)$ so that the frequency enters in Y both directly and through ϵ_r and effects in the pass bands effectively increase ϵ_r and thus the admittance Y. The latter will also show subsidiary maxima and minima arising from the oscillatory terms in (11).

In figure 4, $|\epsilon_c/\epsilon_0|$ calculated from (10) is plotted against ω_H/ω_0. We see that (10) is

$$\epsilon_\perp/\epsilon_0|_{k=0} = \epsilon_c/\epsilon_0 = 1 - \omega_p^2/(\omega_0^2 - \omega_H^2), \tag{17}$$

and when

$$\omega_0^2 = \omega_p^2 + \omega_H^2 = \omega_T^2,$$

i.e. at the upper hybrid frequency, ω_T, $\epsilon_c \to 0$ so that the admittance (which is proportional to the received current when the applied voltage is kept constant), goes to zero. In addition when $\omega_0 = \omega_H$ then

$$\epsilon_c \to -\infty \quad \text{i.e.} \quad |\epsilon_c/\epsilon_0| \to \infty$$

and the admittance becomes infinite.

(2) *Variable grid separation* (ω, ω_H, ω_p *constant*). The electric field, at distances greater than a few Debye lengths from the antenna, may, as we have seen, be expressed as a cold plasma field (effectively infinite wavelength in the present context) plus, in the appropriate frequency pass band of figure 2, the electric field of one or two propagating Bernstein modes. For the case of waves with wavenumbers k_1 and k_2 this superposition produces an electric field in the region between the grids of the form

$$E(x,t) = E_0[\alpha\, e^{i\omega t} + \beta\, e^{i(\omega t - k_1 x)} + e^{i(\omega t - k_2 x)}],$$

where α and β represent the respective amplitudes. Since the two cyclotron waves concerned have group velocities in the same direction, the numerical values of k_1 and k_2 are of opposite sign.

The amplitude, A, of the signal is then found to be dependent on x and given by,

$$A^2(x) = [(1+\alpha^2+\beta^2) + 2\alpha\beta\cos k_1 x + 2\alpha\cos k_2 x + 2\beta\ \cos(k_1 - k_2)\, x]\, E_0^2. \tag{18}$$

Typically $|k_1| > |k_2|$ and $\alpha > 1 > \beta$. Although α and β are here assumed not to be functions of x, in an experiment they normally depend on x. This functional dependence is, however, not harmonic and hence as the separation between transmitting and receiving antennae increases, the received signal is periodically modulated by the $\cos k_1 x$, $\cos k_2 x$ and $\cos(k_1 - k_2)\, x$ terms in (18). Therefore, in principle, the electron Bernstein mode wavenumbers are directly measurable.

The kind of electric field excited as a function of x, resulting from the interference of the components may be seen from (9). For simplicity, consider $\omega_0 < \omega_T$, so that k_2 is absent, and x is assumed large enough that damped contributions are negligible. Then E is of the form

$$E(x,t) = E_0(a\, e^{i\omega t} + e^{i(\omega t - kx)}), \tag{19}$$

where a is the ratio of the amplitude of the capacitively coupled wave and the Bernstein mode. The potential relative to the electrode takes the form

$$A(x) = -E_0[ax + (1/k)\sin kx - (i/k)\,(1-\cos kx)]\, e^{i\omega t}. \tag{20}$$

(Note that in addition to the $\sin kx$ term there are quadrature components, ϕ, introduced at this stage into the voltage (see below).) The amplitude is given by

$$A^2(x) = E_0^2\left[a^2x^2 + \frac{2}{k^2} + \frac{2}{k}\left(a^2x^2 + \frac{1}{k^2}\right)^{\frac{1}{2}} \sin(kx - \phi)\right], \tag{21}$$

in which $\phi = \arctan\dfrac{1}{kax} = \arctan\dfrac{(\text{cyclotron voltage amplitude})}{(\text{cold amplitude})}$. Thus ϕ is small, since, in general, warm plasma effects are small perturbations superimposed on the cold plasma effects.

Experimentally, we excite the modes using an r.f. signal. As a small high impedance, voltage-detecting probe moves away from a source driven by a constant current $\dot{\rho}_{ext}$, we expect to find, assuming ϕ is small or constant, amplitudes fluctuating according to the sine curve in (21) with voltage maxima separated by a distance δx, where

$$\delta x = 2\pi/k = \lambda,$$

i.e. the maxima are separated by one cyclotron wavelength (rather than $\frac{1}{2}\lambda$, as in the usual standing wave case). Finding this wavelength for a given ω_0 by moving a detecting probe enables the dispersion relation to be found

The superposition of one Bernstein mode on the capacitively coupled signal is illustrated schematically in figure 5*a* (corresponding to (19)). As x increases, the signal amplitude oscillates.

In practice, the oscillation will be superimposed on a signal which decreases gradually in amplitude with increasing x. Figure 5*b* shows the more complicated case when two modes are excited simultaneously. Again the combined oscillations corresponding to the $\cos k_1 x$, $\cos k_2 x$ and $\cos (k_1 - k_2) x$ terms in (18) will be superimposed on a decreasing signal level as x is increased.

Thus the voltage obtained by a small high impedance probe is a measure of the impedance for sources driven by a constant current and the impedance will then fluctuate as k or x is varied in accordance with (20) above, or, for $\omega_0 > \omega_H$, in a way which corresponds to the superposition of two expressions similar to (20). Similarly, the received current (in a low impedance detector) when the system is driven by a constant voltage, will represent plasma admittance changes (see below) and any oscillating component is related to Bernstein modes propagating between probes.

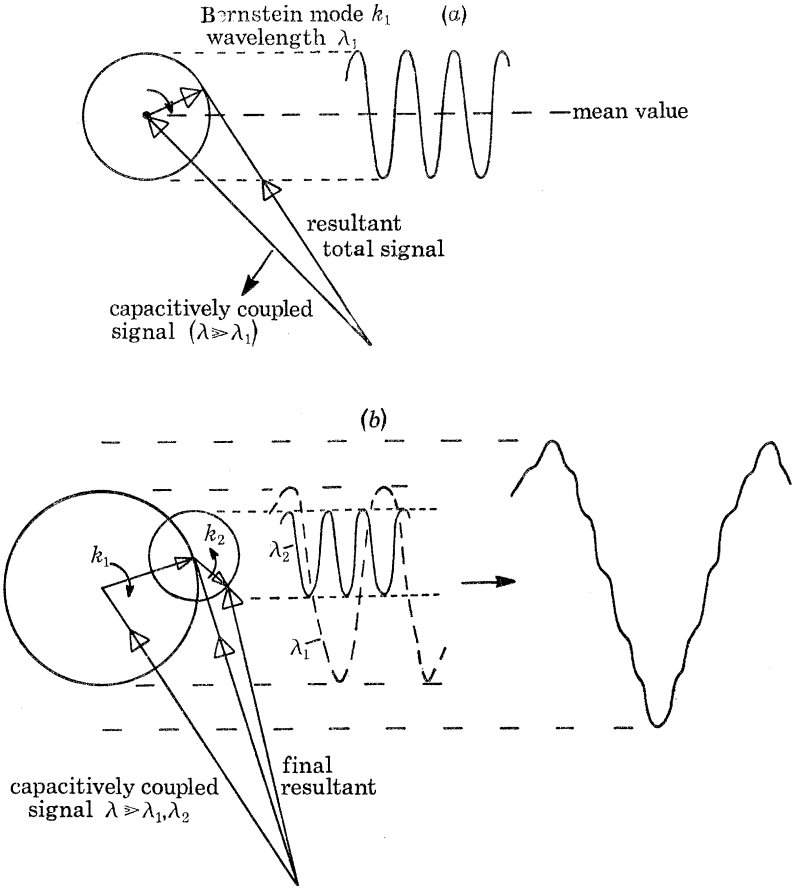

FIGURE 5. The electric field in the space between two antennae in a plasma when an r.f. signal is applied to one of them will consist of the electromagnetic signal (virtually relatively infinitely large wavelength) and one (*a*) or two (*b*) slow propagating, Bernstein mode signals. Since they all originate from a common source, there will be phase coherence and the interference-like pattern in the intervening space may be 'sampled' by moving one probe away from the other and measuring the current to it when a constant voltage is maintained between them, i.e. by measuring the admittance of the probe-plasma-probe circuit. Note k_1 and k_2 have opposite phase rotation directions.

(*b*) *Cylindrical wire antennae immersed in a plasma*

So far we have considered plasma admittances calculated for the case when the source structures corresponded to two infinite plane grids. Mantei (1967) has shown that the admittance when two infinite cylindrical conductors are immersed in the plasma is very similar to the case of the infinite

grid. This confirms that the admittance fluctuations are caused by the plasma itself through the zeroes of $\epsilon_\perp$ in (4) and not by the particular antenna geometry.

The geometry considered by Mantei (1967) corresponds more closely to the situation pertaining in our experiments in which the antenna was simply a small wire. The normalized plasma impedance then reduces to

$$Z(\omega) = -\left(\frac{1}{\omega C_0}\right)\left(\frac{i\epsilon_0}{\ln(2x_0/a)}\right)\int_0^\infty \frac{J_0(k_\perp a) - J_0(2k_\perp x_0)}{k_\perp \epsilon(k_\perp, \omega)}\,dk_\perp, \tag{22}$$

which can be compared with (11). In this expression J_0 is a Bessel function, $2x_0$ is the wire separation, a is the radius of the wire, C_0 is the vacuum capacitance between parallel conducting cylinders (appendix B).

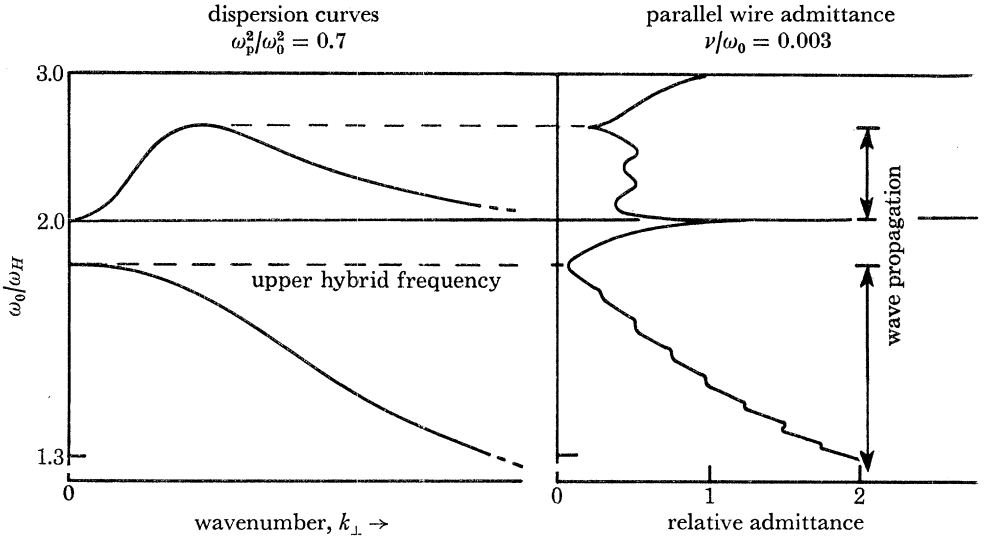

FIGURE 6. (Right). The admittance per unit length between wires immersed parallel to a static magnetic field, $\boldsymbol{B}_0$, in a plasma with a low electron-neutral collision frequency, ν, (computed by Mantei 1967). On the left the corresponding dispersion curves are sketched. The enhanced admittances near the gyroharmonics as well as the subsidiary oscillatory components of the admittance in the region of propagating Bernstein modes are clearly seen. The admittance null (cf. figures 4 and 8) at the upper hybrid frequency is also shown.

Mantei's results are redrawn in figure 6 to show the relation of the admittance to the propagation bands. Admittance maxima in the pass bands above the gyroharmonics and below ω_T are again caused by a minimum voltage across the plasma, due to the presence of an even number of cyclotron half wavelengths between antennae. Between admittance peaks then, ω_H/ω_0 has changed to allow one more (or one fewer) cyclotron wavelength to be accommodated. The series representation of (11) clearly lends itself to an understanding of the contributions of the different modes to the plasma impedance. No corresponding series representation of the integral in (22) appears to be available.

5. Experimental background

The earliest laboratory observations of noise emissions at right angles to $\boldsymbol{B}_0$ at the electron gyroharmonics together with subsequent extensive work near these, and other plasma characteristic frequencies, have been reviewed by Crawford (1969) and by Dreicer (1969) and in references cited therein. The first attempts to make measurements explicitly on the Bernstein modes were by Crawford, Kino & Weiss (1964) and by Harp (1965) who used probes placed

inside plasma columns of fairly uniform density. Subsequently the group velocities of the waves were measured by Crawford *et al.* (1967) who used a pulse delay technique; Mantei (1967) made extensive observations of plasma admittances.

All these experiments were done at a fixed frequency and the dispersion parameter $\Omega = f/f_H$ was varied by altering the magnetic field. Unfortunately in discharges of the type used, this results in a change of plasma density and a quantitative comparison with the theoretical dispersion curve is difficult. The work presented in this paper followed preliminary unpublished work by the author at the NASA Ames Research Center in 1964 and is based on the idea of an interference type experiment using a moving probe so that the plasma parameters were constant (Andrews 1969; Thomas, Andrews & Hall 1970; Thomas, Andrews, Hall & Phelps 1971). The work was extended by Hall & Landauer (1971).

Apart from the fundamental interest in verifying the dispersion equation (3) the waves may lead to ways of measuring plasma parameters that are independent of sheath effects. Similar experiments were carried out independently by Leuterer (1969) and Clinkemaille (1970). Gonfalone (private comm.) has developed similar experiments in relatively large plasma chambers so that the direction of the ambient magnetic field could be changed by rotating the field coils.

6. The experiments

Experiments have been carried out in the oxide-cathode discharge tube shown in figure 7. The gas used is argon at a pressure, p, of 13–130 mPa, which, at an operating frequency of typically 500 MHz gives a collision/wave frequency ratio of the order of 0.001. The plasma column is about 5 cm diameter, many times the electron gyroradius at the magnetic field strengths employed, and has a density of 10^9–10^{10} electrons/cm^3. The type of antenna probe may be changed,† and both are movable; one may be extracted at a constant rate by means of an electric motor. A signal of frequency in the range 450–1000 MHz is applied to one probe. This signal is amplitude modulated at 1000 Hz and input at a constant voltage level. The modulation amplitude is about 0.1 V. The current received by the second antenna is monitored by a narrow band heterodyne detector and displayed on an X–Y recorder. The gyrofrequency f_H may be held constant, or swept from zero to 700 MHz by altering the current in the field coils (figure 7). The magnetic field was calibrated by using a Hall probe gaussmeter. It is constant to 1 % over ± 4 cm near the probes and along the tube axis and is substantially independent of radial position. An earthed anode mesh isolates the discharge chamber from fluctuations near the cathode and provides a relatively stable plasma. In this discharge, the Debye length is fairly large (*ca.* 0.2 mm). The smallest antenna diameter was 0.2 mm. It is unlikely therefore that Bernstein mode wavelengths shorter than this are observable. In fact, the sheath size will limit this to an even greater value, and in practice, the shortest wavelength observed experimentally was about 0.8 mm. A Langmuir probe was used to measure radial electron density and temperature profiles and to monitor the noise level in the plasma.

(*a*) *Plasma admittances: fixed antenna separation*

Assuming that stray impedances to grounded electrodes are small and that sheath thicknesses are such that their capacitive reactances are small, then fluctuations in the received current in a low impedance detector when a constant antenna driving voltage is applied represent plasma

† A number of different antenna configurations were tried. Best results were obtained with a ferromagnetic nickel wire transmitting antenna about 2 cm in length with a similar earthed wire mounted about 1 mm in front of it.

admittance changes and any oscillating component is related to plasma waves (Bernstein modes) propagating between probes.

Figure 8 shows the received signal, representing the relative plasma admittance, as f_H is swept over three ranges of the ratio f_H/f. The admittance has the same general shape as the inter-electrode capacitance illustrated in figure 4 with which figure 8 should be compared, i.e. it is approximately related to the modulus of the cold plasma permittivity given by (17) and therefore

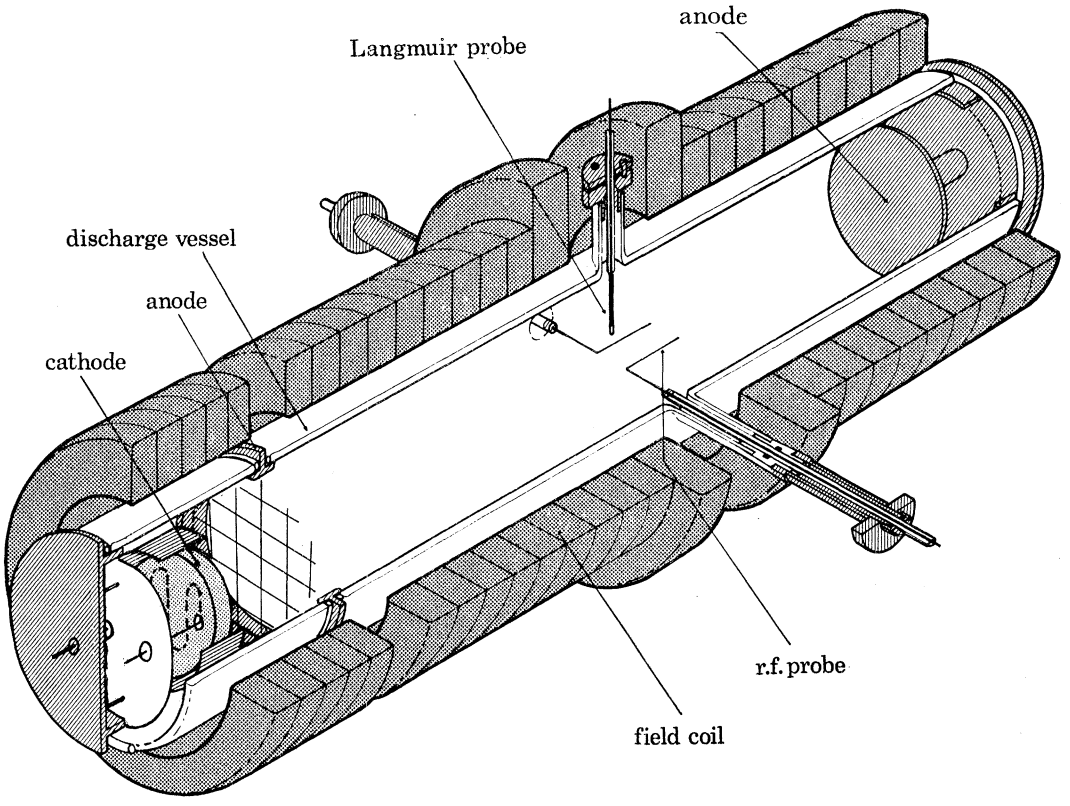

FIGURE 7. Cut-away drawing of the discharge tube fitted with an indirectly heated oxide cathode. The operating gas (argon) is fed in through a port below the probes. The system is continuously pumped.

falls to a minimum at the upper hybrid frequency, ω_T, where the plasma presents its highest impedance. This signal null, clearly observable in all three curves, occurs at

$$\omega_T^2 = \omega_p^2 + \omega_H^2$$

and may, for a known magnetic field, be used to indicate ω_p and hence plasma densities regardless of sheath effects. The infinite admittance at $f_H/f = 1$ is particularly clear in curve *c* of figure 8. The warm plasma effects are superimposed on this overall shape and consist of large admittance enhancements near the gyroharmonics with subsidiary periodic admittance 'ripples' as discussed in § 4 (*a*) (1). Within the accuracy of the experiment, the admittance peaks (seen here to the 20th harmonic) do fall exactly at the gyroharmonics.

An interesting observation is that of the apparent increase in admittance (figure 8*b*), (with warm plasma oscillations superimposed) which reaches a peak between ω_H and ω_T. In this region, cold plasma theory predicts that the plasma is inductive (ϵ_c negative). The observations

show characteristics (Andrews 1969) of a series resonance effect due to capacitive sheaths surrounding the antennae.

In theory, the dispersion curve could be constructed from the admittance oscillations obtained as f_H (and hence k) is swept through the regions where cyclotron waves propagate. As discussed, in moving from one maximum to the next for $\omega_0 < \omega_T$, kx changes by 2π while it is known that $k = 0$ at f_T and at gyrofrequency harmonics. *In practice, the method has the disadvantage that the plasma density also changes as f_H is swept.* To obtain dispersion characteristics, it is much more satisfactory therefore to vary the probe separation continuously at different operating frequencies for a fixed discharge current and magnetic field.

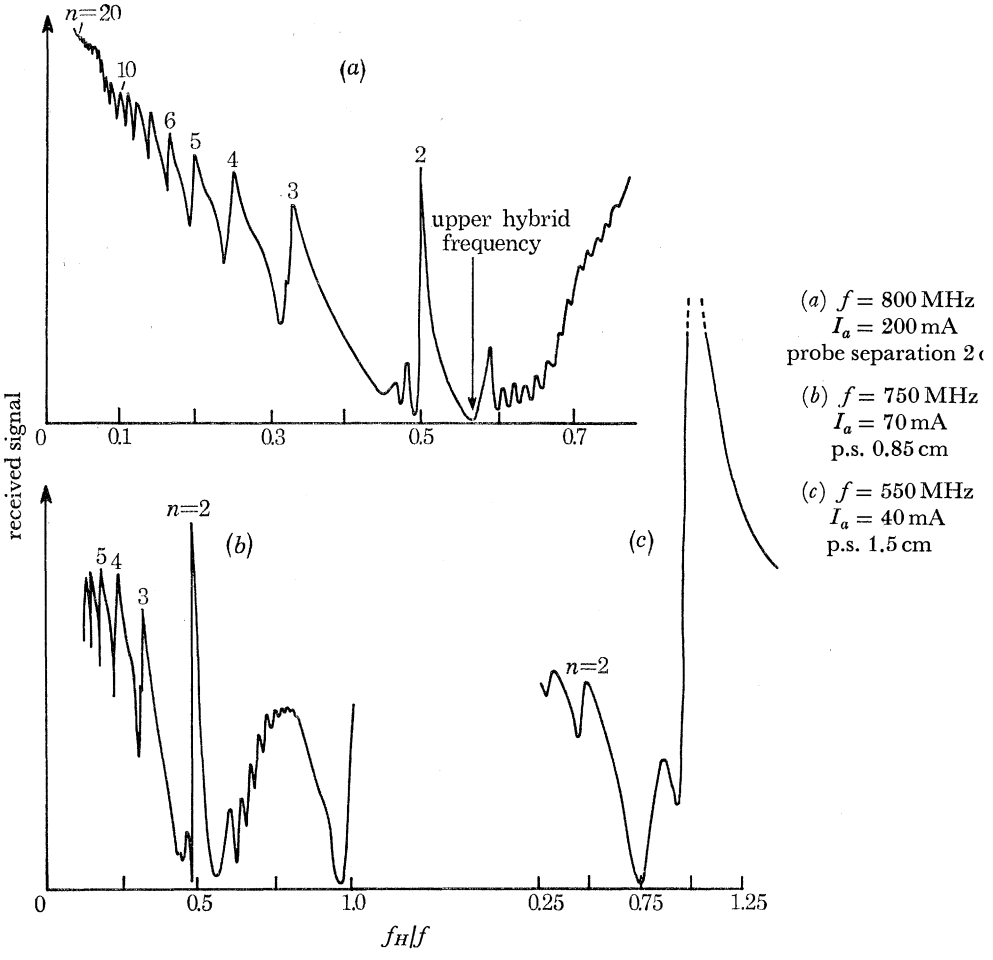

FIGURE 8 (a, b, c). The signal received (which is proportional to the admittance for a constant driving voltage) when transmitting between two antennae in the plasma when the field coil current is changed to vary f_H, keeping the applied frequency, f, constant in each case. These curves should be compared with the general form of figure 4. Hot plasma effects are clearly visible and take the form of (1) enhancements of the admittance in the vicinity of the electron gyroharmonics (visible up to the 20th harmonic), (2) subsidiary admittance oscillations. The null at the upper hybrid is clearly visible in curves (a) and (c). The plasma represents zero impedance at $f_H/f = 1$ curves (b) and (c). Note also the 'anomalous' increase in admittance between $f_H/f \simeq 0.5$ and 1.0 in curve (b). This is thought to be a sheath resonance effect (see text) and may provide a useful way of determining sheath characteristics. The anode current, I_a, is different in each case. The pressure, p, is *ca.* 27 mPa.

(b) Plasma admittances: antenna separation varied (ω, ω_H, ω_p constant)

For $\omega_0 < \omega_T$ the impedance or admittance between probes has an oscillatory component as given by (21) and the wavelength of the Bernstein mode may then be measured directly as the separation between consecutive maxima or minima. Figure 9 shows records of admittance as a function of probe spacing, and demonstrates well the effects of the interference of the capacitive

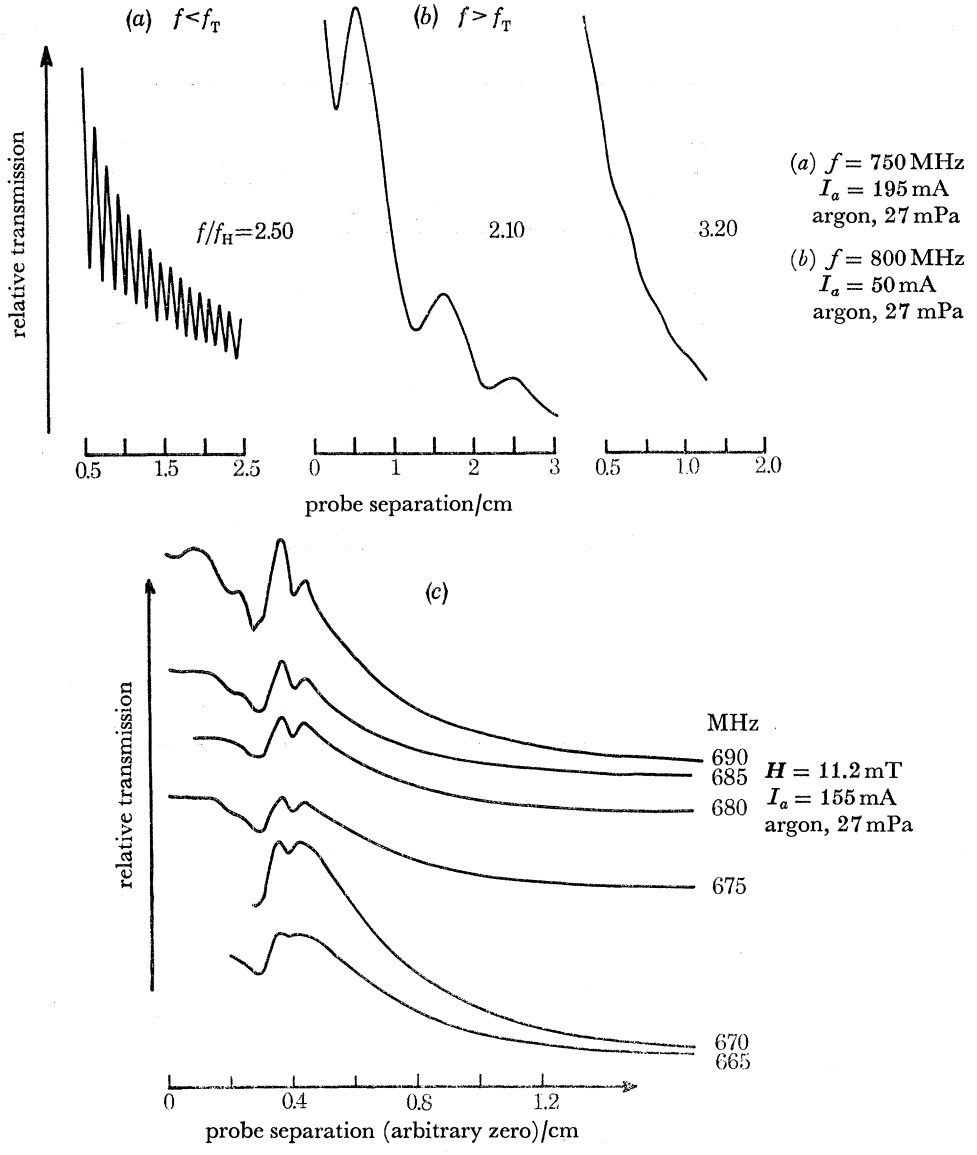

FIGURE 9 (*a*, *b*, *c*). The received signal for a given ratio of the applied radio frequency and the ambient static magnetic field when the antenna separation is increased. The oscillatory response arises from the interference of a propagating Bernstein mode signal with the capacitively coupled signal (cf. figure 5).

and Bernstein mode signals. The left hand curve (*a*) corresponds to the case where $f < f_T$, i.e. to the excitation of a single k mode. Similar curves for $f > f_T$ are shown in the same figure (*b*). In general, in this case, there are two propagating Bernstein modes k_1 and k_2 but, in practice, the high k (short wavelength, low group velocity) mode, k_1, is often highly attenuated with respect to the mode at k_2 because of the greater effect of collisional damping at the lower group velocity and

this is the case for the curves labelled (*b*). Figure 9*c* however is an example in which the short wavelength mode is clearly visible.

Examples of experimental dispersion curves obtained by means of the interference technique are given in figure 10*a*, *b* for particular sets of plasma parameters. The experimentally derived points are plotted on the same graphs as the theoretical curves obtained from (3). The plasma density required for (3) was obtained from a measurement of the upper hybrid transmission null at ω_T and from a knowledge of the magnetic field value. The parameter r, the gyroradius of an

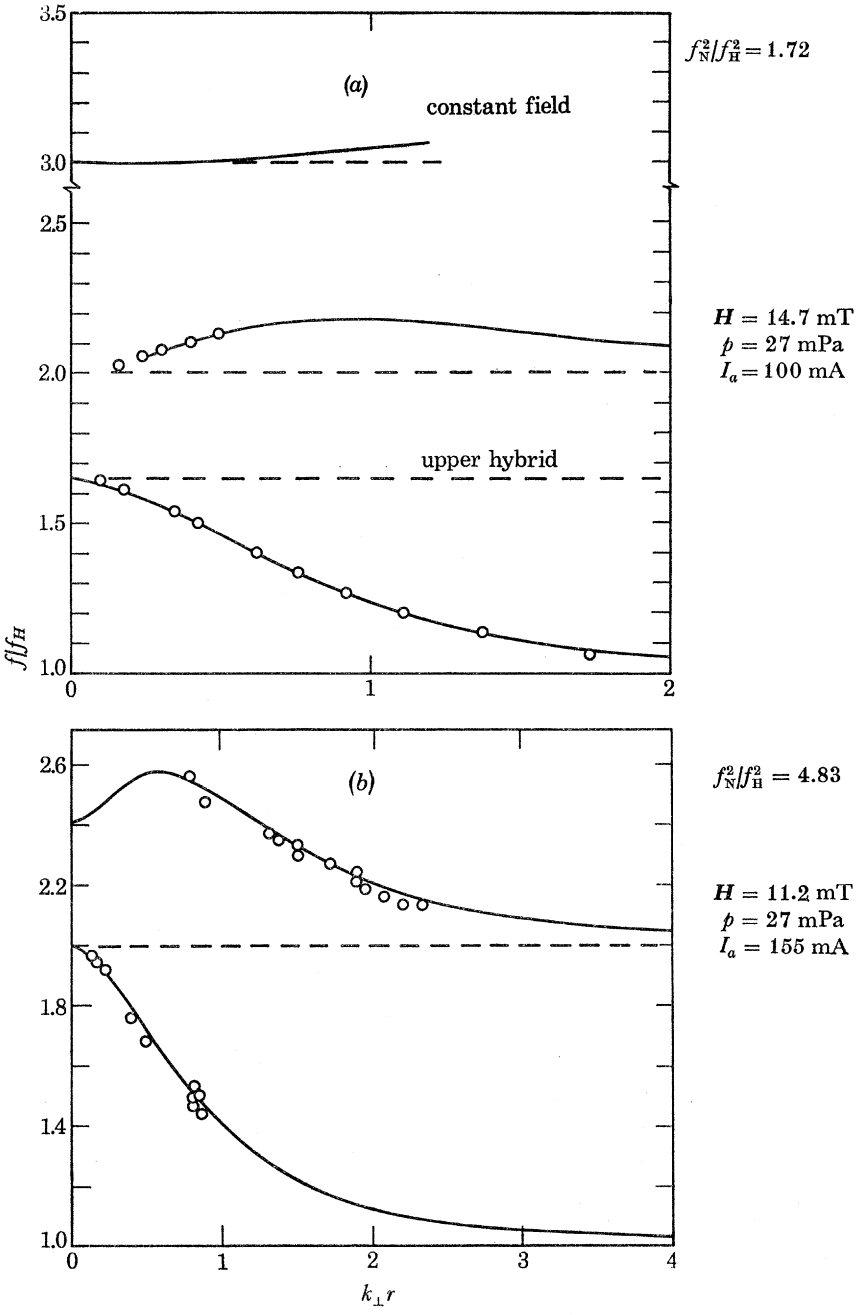

FIGURE 10 (*a*, *b*). Comparison of theoretical dispersion curves with experimental measurements for the Bernstein modes (see text). ooo, experimental points; ——, theory.

'average' thermal electron was adjusted to give the best fit between experiment (which measures $k_\perp$ directly as described above) and the theoretical curves plotted with $k_\perp r$ as abscissa. Now r is defined from

$$r^2 = KT/m\omega_H^2,$$

in which K is the Boltzmann constant and T and m are the electron temperature and mass respectively. For the case in figure 10*a*, the electron temperature is 3.3 eV (*ca.* 40 000 K).

The ultimate wavelength detectable in the experiment is one comparable to the 'collector' size, i.e. the diameter of the probe-sheath combination, which was determined mainly by the Debye length. This combination was estimated to be about 0.8 mm, and while wavelengths down to this size were measured, many of the short modes are predicted to be below this limit.

7. Plasma wave radars

The recorded signals often referred to in the literature on ionospheric physics as plasma 'resonances' or 'spikes' were first observed in an experiment in which a radio frequency transmitter was carried on board a rocket fired into the E region (Knecht, Van Zandt & Russell 1961) (figure 11).

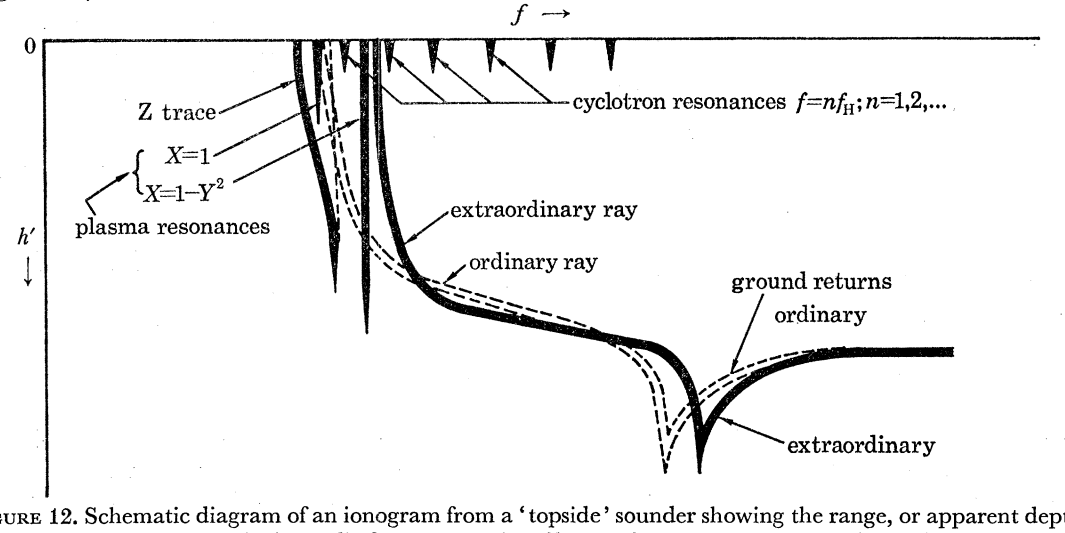

FIGURE 12. Schematic diagram of an ionogram from a 'topside' sounder showing the range, or apparent depth, h', below the satellite at which a radio frequency pulse of known frequency was reflected. The 'spikes' excited at a number of plasma characteristic frequencies are indicated. These returns are caused by slowly propagating plasma waves which are quite different in character from the electromagnetic wave returns labelled ordinary and extraordinary ray in the diagram (see text).

Later, when a variable frequency pulsed radar was carried aboard the 'topside sounder' satellite Alouette I, which was launched in September 1962, it was realized that similar signals occurred at a number of plasma characteristic frequencies (table 1; figures 12, 13). Early explanations of these effects involved the idea that waves were being excited by the radio frequency signal applied to the antenna while it was immersed in the plasma and that these waves were of a kind (unlike ordinary electromagnetic waves) that travelled sufficiently slowly that they were able to 'keep up' with the satellite. In other words their group velocities were o the same order as the satellite velocity (*ca.* 10 km/s), some four orders of magnitude lower than the free space electromagnetic wave velocity. As a result, two kinds of signals were generated on the topside ionogram – the usual radar echo return corresponding to the reflexion of the pulses of electromagnetic waves with time delays of up to several milliseconds and the 'resonances' or

'spikes' corresponding to 'plasma ringing' effects caused by the reception of the slow waves recorded over an apparently wide range of time delays extending from a few milliseconds to virtually zero. We now know that such ideas (involving simply the matching of satellite and group velocities) are inadequate to describe the detailed structure displayed in the radar returns and that the so-called resonance spikes can be better understood (McAfee 1968, 1969*a*) as arising from the reception of plasma waves excited by the r.f. signal applied to the spacecraft antenna and reflected close to the satellite by an electron density gradient and the associated refractive index changes with distance above or below the vehicle.

It therefore becomes important to carry out ray tracing in hot magnetoplasmas in order to determine the paths followed by the various kinds of excited plasma waves and to determine which of these paths, if any, are such that they cross at some later time, the track of the satellite once more – for it is the interception of these slow waves by the vehicle – after a relatively long time delay (which can be calculated) – that accounts for the 'resonance spikes'.

A research program involving ray tracing in hot magnetoplasmas was started to determine the feasibility of a plasma wave radar since it is clear that plasma waves from a stationary source (e.g. an antenna immersed in a laboratory plasma or a geostationary satellite) may, after a time, be returned to the source and this has been confirmed following detailed three-dimensional ray tracing carried out first by M.T.C. Fang and later by R. Buckley at Imperial College. We shall return to this work later in the paper and will describe at that stage, the ways in which plasma waves and plasma wave radars might be of value in laboratory and space plasma diagnostics. In addition we shall postpone a discussion of the basic ideas involved in such ray tracing projects and of the problems encountered in determining the refractive index in an economical way (i.e. of selecting appropriate mathematical models to describe the relevant hot-plasma properties) until a presentation has been made qualitatively of the nature of the ray paths followed. This is best illustrated with the aid of the Poeverlein construction as indicated by McAfee (1968).

The Poeverlein construction

Schematic polar plots at fixed frequency of refractive index, μ, against the propagation direction, θ (angle between $\boldsymbol{k}$ and $\boldsymbol{B}$), are shown in figure 14.† The Earth's magnetic field direction is along AOB so that α is the dip angle and the electron density gradient is vertical. The curves marked (1)...(4) represent cross sections in the zx plane of these refractive index 'surfaces' which are symmetrical about the field direction and refer to increasing values of the plasma frequency, ω_p, i.e. to decreasing values of refractive index with depth below the satellite for $\omega > \omega_p > \omega_H$, where ω is the frequency and ω_H the electron angular gyrofrequency. In the case of a vertical gradient of electron density, i.e. of refractive index, μ, Snell's law states that the horizontal component of the refractive index, μ_H, is constant along a ray path corresponding to a vertical line in figure 14. Suppose the satellite is at a level where ω_p is such that the refractive index corresponds to the point P_1 on curve (1) in figure 14. The direction of the group velocity is normal to the refractive index surface, as shown, and the ray direction is left and downwards into a region of lower μ, corresponding to, say, the point P_2 on curve 2 on the vertical line P_1P_2 (since μ_H is constant). At P_2, the direction of the normal to the refractive index is more towards the vertical and so the ray turns slightly to the right but continues downwards and to the left to a level

† Note that the curves (1) etc. in the upper part of figure 14 represent (μ, θ) for a given frequency and plasma. If the plasma density is assumed to vary in space, refractive index 'surfaces' for different plasma parameters relate to different positions in the plasma.

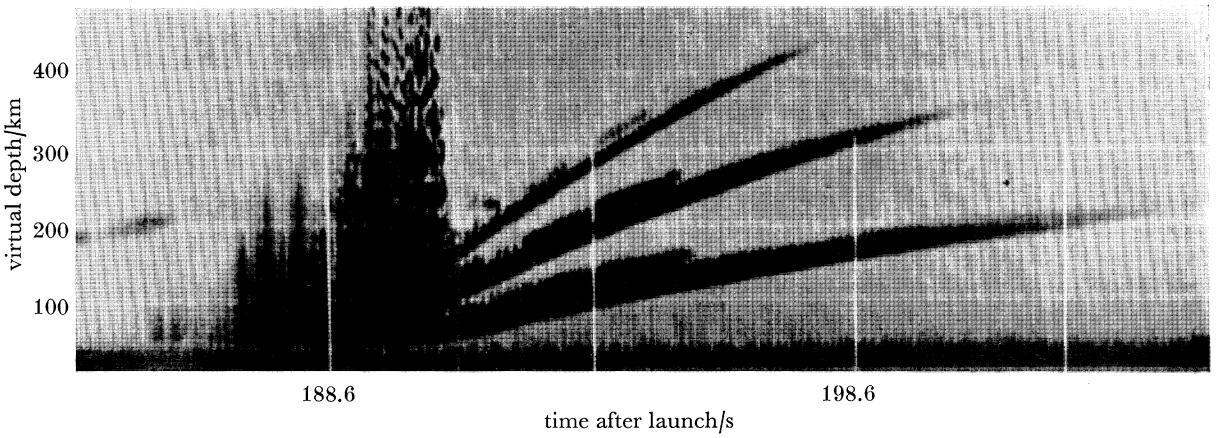

FIGURE 11. Early observations of a 'plasma resonance spike' excited by a rocket-borne transmitter immersed in the ionospheric plasma. The time delay, or vertical depth of reflexion, of signals near a frequency of 5.97 MHz is recorded as a function of flight time (after Knecht *et al.* 1961). Record made 24 June 1961, 18h17 LMT.

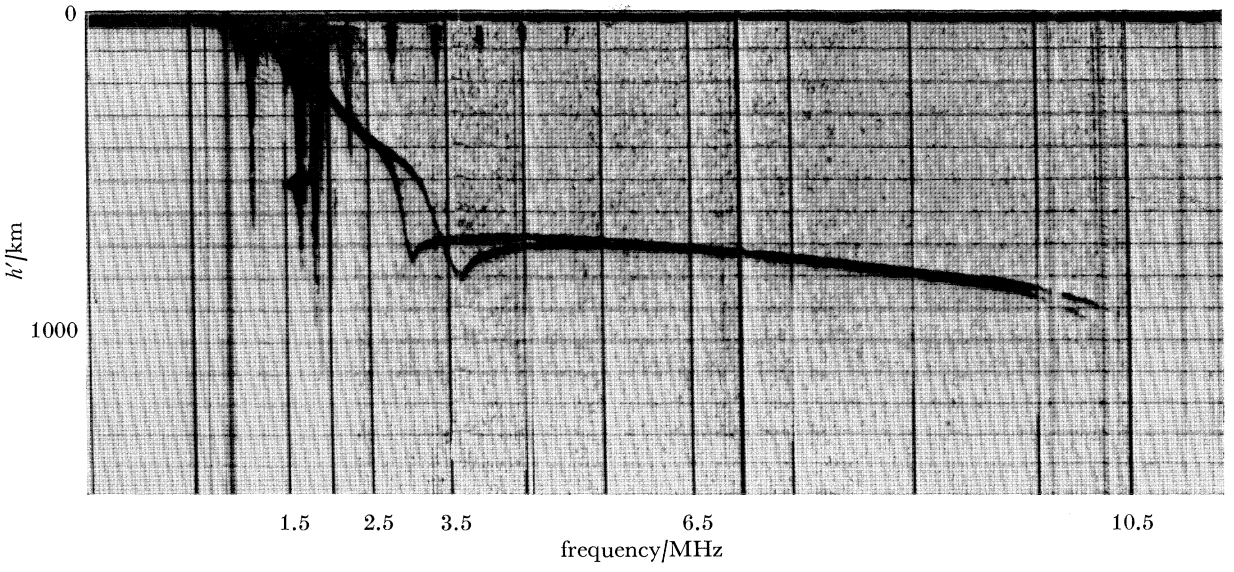

FIGURE 13. An actual Alouette I topside ionogram recorded at low latitudes. The ordinate is the virtual depth of reflexion of the signal. The vertical lines are frequency markers. Both the electro-magnetic wave returns and plasma wave returns are clearly visible (cf. figure 12).

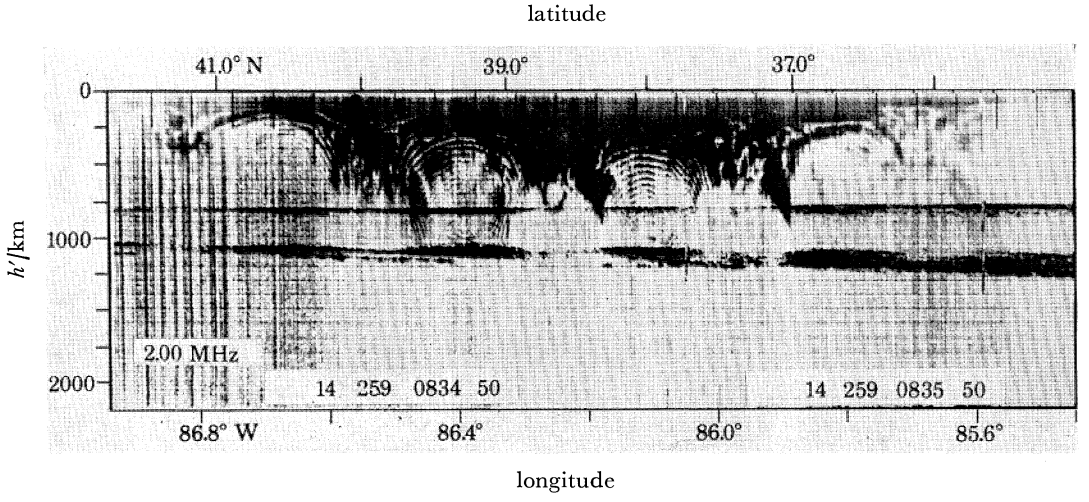

FIGURE 15. Part of a film record from the Explorer XX satellite in which the virtual depth of reflection of a transmitted pulse (here 2 MHz) is recorded as a function of time. The 'resonance' or plasma wave signals appear as a continuous echo modulated in virtual depth by the roll motion of the satellite antennae. The interference pattern arises from the beating of two plasma waves of different wavelengths. (15 Sept. 1964/0834Z/0248 LMT, $f_H = 1.02$ MHz, satellite height = 968 km).

(*Facing p.* 212)

where μ corresponds to P_3, say. The normal at P_3 points to the right and so the ray is now moving to the right though still downwards. At the level corresponding to P_4, the group velocity direction is horizontal and to the right, corresponding to the level of reflexion. Continuing to apply this procedure, known as the Poeverlein construction, gives the complete ray path as shown in the lower sketch in figure 14. Beyond P_4, the ray is moving upwards and encountering increasing

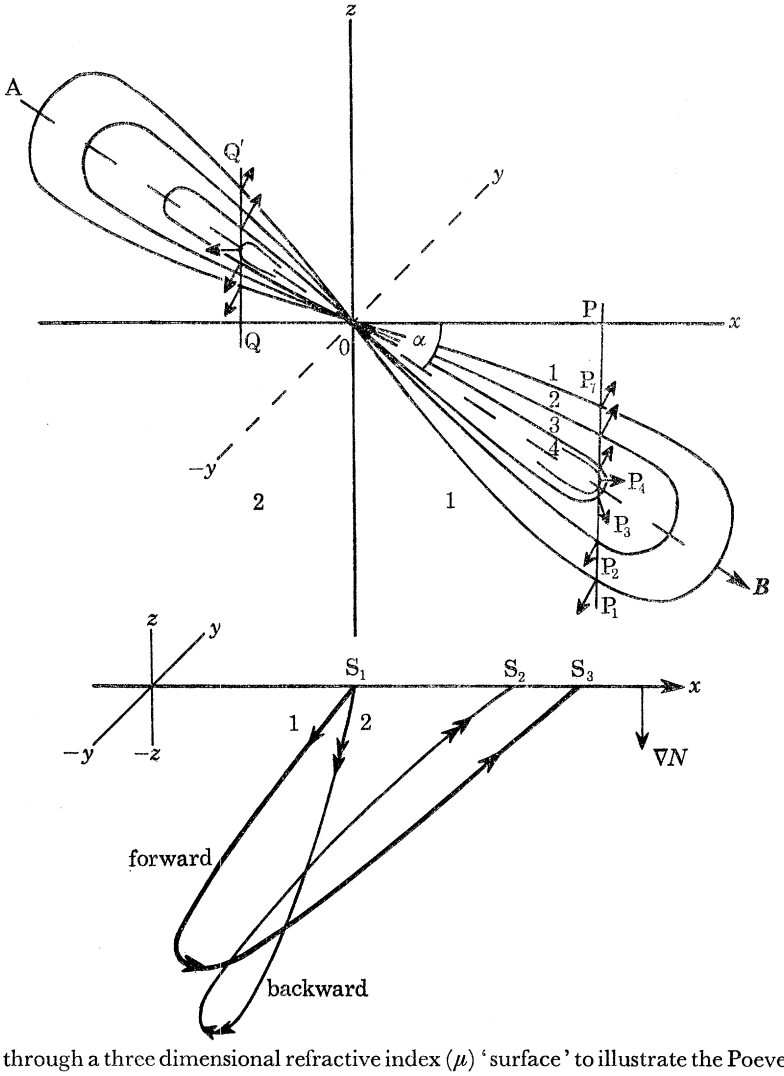

FIGURE 14. Section through a three dimensional refractive index (μ) 'surface' to illustrate the Poeverlein construction (see text). The group velocity (and ray direction) associated with a particular value of μ, at some point P, is the normal to the refractive index surface and is indicated by an arrow. Clearly, very large changes in the group velocity direction can occur for small changes in μ and θ. Ray paths for a satellite moving in the x-direction in the plasma at a level corresponding to P_1 and P_7 are shown. The theoretical work described, however, applies to any satellite trajectory.

values of μ until it reaches P_7, corresponding to the original level of the satellite. If, in the time t_1 taken to traverse the path marked 1 in the plasma, the satellite has moved from S_1 to S_3, then the ray will be received with a delay time, t_1 (forward ray). The refractive index surfaces also extend to the third quadrant (figure 14) and give rise, by the same construction, to the ray path marked 2 (the backward ray) which is moving in the opposite direction to ray 1 at reflexion. The backward ray corresponds to a slightly different frequency (finite transmitter pulse lengths give, typically, 20 kHz frequency width for the carrier band, i.e. for a single pulse, a range of frequencies, i.e. of

$f_N + \Delta f$ values (see later) are present and a corresponding range of k modes are excited over a range of values of θ_0, the initial propagation angle) and so the distances OP and OQ are not the same and the curves in the fourth quadrant are slightly different from those in the second quadrant because of the dependence of refractive index on frequency and on θ. This ray intercepts the satellite track at S_2 and so would not be picked up by the satellite which has reached S_3 in the time t_1. McAfee, however, found that the receiver bandwidth was sufficient, in the case of propagation at frequencies just above ω_p, for two signals of slightly differing frequency and initial propagation angle corresponding to forward and backward modes,† like those illustrated, to have the same time delay, t_1, and hence to arrive at S_3 together. In these circumstances, the satellite receives two signals at slightly different frequencies from a common source (the transmitter) so that there is phase coherence between the two waves received and interference takes place. Figure 15 is an example showing the bands of maximum and minimum signal as well as modulation associated with the spin of the satellite.

Typical ray trajectories for frequencies near the plasma frequency ω_p show penetrations to real depths up to about 1 km below the level of the satellite. Time delays of up to about 1.5 s but, typically, a few hundredths of a second, are observed confirming that slow waves are involved. The transmitted pulse will excite a whole range of wavenumbers which will have different values for the angle, θ_0, between the wavevector and the magnetic field. In figure 16 the time delay for plasma waves of three different frequencies $f_N + \Delta f$, are plotted against the average velocity, $V_s = \Delta x/t$, along the satellite track, for wavenumbers with different values of θ_0, where Δx is the distance travelled in the x-direction by the ray during time t. For example, the lower curve shows that a plasma wave of frequency $f_N + 2$ kHz, i.e. 1.5 MHz would be received by a satellite travelling at approximately 10 km/s after a delay of about 1.6×10^{-2} s. A wave of the same frequency but a different value of $\boldsymbol{k}$ and of θ_0 would be returned to the source ($V_s = 0$ km/s) after about 1.4×10^{-2} s. Thus a signal would be returned to a moving, or, to a stationary source, after a measurable time delay, confirming the basic feasibility of a plasma wave radar. The intersections of the curves of figure 16 with a series of vertical lines provide plasma wave ionograms (delay time against frequency), the intersection of the vertical line with the abscissa giving the satellite velocity appropriate to the reception of the particular ionogram. The ordinate gives the plasma wave ionogram for a geostationary satellite or for a stationary probe in a laboratory plasma. (Note that the criterion is that the probe must be stationary with respect to the plasma – the plasma itself may of course be moving.) In practice, allowance must also be made for a Doppler shift in frequency when moving satellites are considered. Figure 17 shows a plasma wave ionogram for conditions appropriate to a geostationary orbit. It should be noted that approximate 'mirror image' type curves exist for the backward ray not plotted in figure 16. For a stationary plasma and stationary satellite these would cross at the same ordinate values. In general, however, two slightly different frequencies would reach the satellite with the same time delay giving rise to the two curves labelled 'forward' and 'backward' in figure 18 which gives the plasma wave ionogram received on a satellite travelling at 7.35 km/s.

The mechanism described above for plasma waves propagating at frequencies just above ω_p is now believed to apply also to those associated with the signals near the upper hybrid frequency (McAfee 1969*b*; Graff 1971) and near the electron gyroresonance frequencies (Thomas, Fang & Andrews 1971; Andrews & Fang 1971).

† For these modes, θ_0 lies in a cone about 30° wide, centred on the direction of $\boldsymbol{B}_0$. For angles greater than this, the behaviour is electromagnetic, i.e. $\boldsymbol{k} \times \boldsymbol{E} \neq 0$.

PHILOSOPHICAL TRANSACTIONS OF THE ROYAL SOCIETY A MATHEMATICAL, PHYSICAL & ENGINEERING SCIENCES

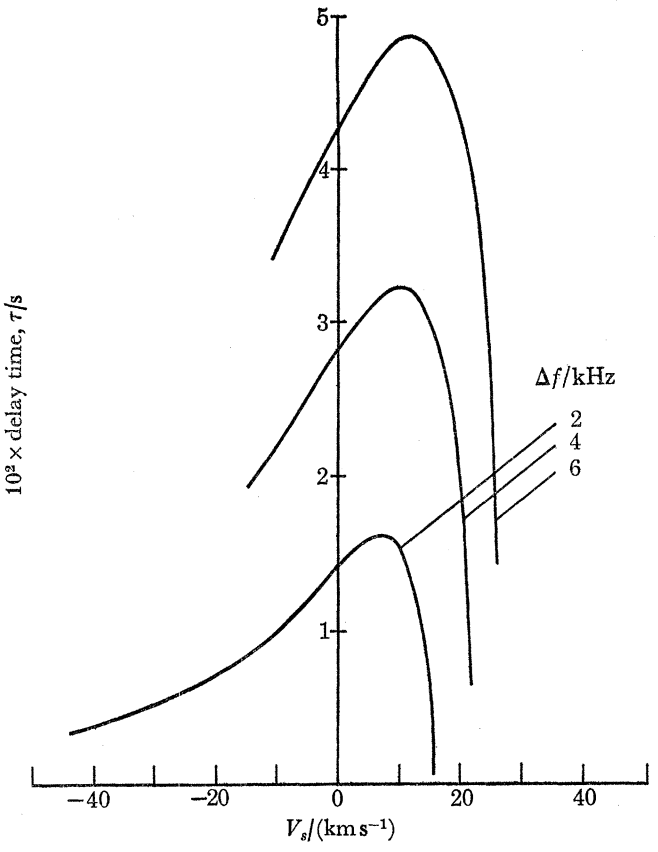

FIGURE 16. Delay time against an average velocity V_s equal to the distance Δx travelled by the wave divided by the travel time for three different values of frequency $f = f_N + \Delta f$, computed for ionospheric conditions ($T = 2000$ K, $f_H = 0.6$ MHz, $f_N = 1.498$ MHz, $H = 4 \times 10^5$ m). The significance of the curves is described in the text.

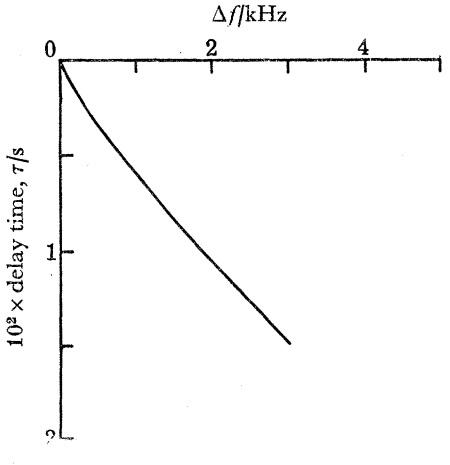

FIGURE 17

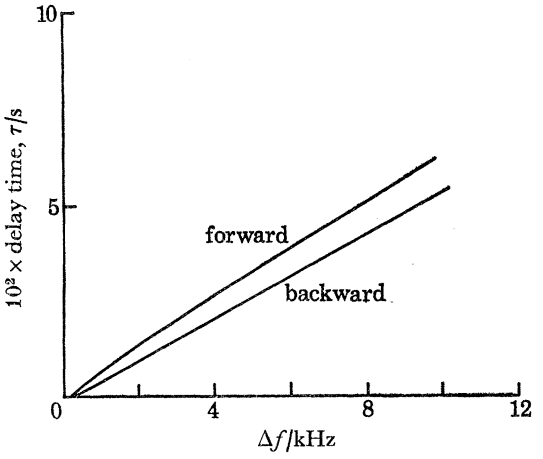

FIGURE 18

FIGURE 17. Computed plasma wave ionogram for a geostationary satellite. ($T = 10\,000$ K, $f_H = 10$ K Hz $f_N = 50$ KHz, $H = 10^6$ m, $\Delta f = f - f_N$.)

FIGURE 18. Computed plasma wave ionogram for a satellite in the ionosphere (satellite velocity 7.35 km/s). Both forward and backward ray traces are shown, see text ($T = 3000$ K, $f_N = 1.498$ MHz, $f_H = 0.6$ MHz, $H = 4 \times 10^5$ m, $\Delta f = f - f_N$).

The ray tracing procedures followed by McAfee and by Fang (1971) were based on detailed computations of a large number of ray paths (using Snell's law) to determine which would intersect the satellite at a particular time, t, after transmission. An important step forward was made by Fejer & Yu (1970) who showed that the method of stationary phase could be applied with advantage.

The method has been applied and extended by Parkes (1974*a*, *b*) and by Buckley (1974) and others. The field produced by a pulsed source at the origin, at the point $\boldsymbol{r}$, in time t may be written (Fejer & Yu 1970; Buckley 1974) in the form

$$\boldsymbol{E}(\boldsymbol{r}, t) = 2\pi \mathrm{i} \int G(\omega, k_x, k_y)\, M(\omega, k_x, k_y, z)\, \mathrm{e}^{\mathrm{i}\phi}\, \mathrm{d}\omega\, \mathrm{d}k_x\, \mathrm{d}k_y, \tag{23}$$

where the phase ϕ is given by

$$\phi = \omega t - k_x x - k_y y - \int_0^z k_z(\omega, k_x, k_y, z')\, \mathrm{d}z', \tag{24}$$

so that $k_z(\omega, k_x, k_y, z)$ is the solution of the dispersion equation $D(\omega, k_x, k_y, k_z, z) = 0$, G is a function depending on the source, and M is an amplitude factor. It is assumed that the transmitted pulse contains a narrow band of frequencies slightly above the local plasma frequency and that for any given ω within this band, plasma waves with various values k_x, k_y of the horizontal wavenumber are excited. The dependence of k_z on z' arises from the variation of plasma frequency with depth below the satellite.

The integral in (23) may be evaluated by the method of stationary phase since the field $\boldsymbol{E}(\boldsymbol{r}, t)$ will have the main contributions from those components which contain values of k_x, k_y and ω such that they make ϕ stationary with respect to changes in k_x, k_y and ω. Thus the values of ω, k_x and k_y which satisfy

$$\frac{\partial \phi}{\partial \omega} = \frac{\partial \phi}{\partial k_x} = \frac{\partial \phi}{\partial k_y} = 0$$

are first found. These represent simultaneous saddle points of the phase ϕ in the complex ω, k_x and k_y planes. The function ϕ is then expanded about the saddle points and the integration carried through. The values of ω, k_x and k_y of the saddle point so determined select that wave packet which has a group path such that it has travelled from the source at the origin to the point (x, y, z) in the time t and this provides the link between the ray-tracing and the stationary phase techniques. Thus the correct ray path to intersect the satellite is determined directly without having to solve the ray paths for a large number of rays.

For $Y < 1$ (i.e. $\omega_\mathrm{p} > \omega_H$ since $\omega \simeq \omega_\mathrm{p}$) the 'thermal' refractive index $\mu_T = v_T/(\omega/k)$ (i.e. the ratio of the electron thermal velocity to the phase velocity of the wave) is computed. A discussion of the use of various plasma models for computation purposes and appropriate references are given by Fang & Andrews (1971). μ_T may be written in terms of its components along Oz and parallel and perpendicular to $\boldsymbol{B}$ and a quartic obtained for μ_{Tz} by eliminating $\mu_{T\parallel}$ and $\mu_{T\perp}$ (Buckley 1974). The procedure is essentially the same as that used in deriving the Booker quartic from the Appleton–Hartree magnetoionic cold plasma formulation. By the use of suitable approximations, Buckley (1974) derives the phase ϕ and sets the partial derivatives to zero to obtain the ray path equation giving t, x, y as functions of z. The satellite path given by $x = v_x t$, $y = v_y t$, $z = v_z t$ is then substituted into the expressions for t, x and y and the frequency ω is Doppler shifted into the satellite rest frame by writing $\omega' = \omega - \boldsymbol{k}\cdot\boldsymbol{v}$. Ultimately it is shown that the two received frequencies may be expressed in terms of a pair of universal functions of a dimensionless time. The analytical expressions for the two frequencies are such that if the received frequencies can be recorded

separately, then both T and the electron density gradient H can be determined whereas, if only the beat frequency $\Delta\omega$ is measurable as a function of time, then only a quantity proportional to the product $\sqrt{TH}$ can be obtained. Similar studies have been made contemporaneously by Parkes (1974*a*, *b*).

8. Summary and conclusions

It has been shown, in a series of experiments with a laboratory plasma, that the electron Bernstein modes may be easily excited and that their propagation characteristics can be readily determined. Good agreement is obtained with the theoretical dispersion relations. In the pass bands below the upper hybrid frequency, the interference experiment gives a rapid method of determining the wavelength of the Bernstein mode without recourse to more difficult pulse experiments involving group velocity measurements. This technique, involving a movable probe at different operating frequencies gives λ directly and is independent of sheath-associated difficulties and of magnetic field-dependent densities. Above ω_T the extraction of both wavenumbers is more difficult but could be resolved, in principle, either by using a Fourier technique, or, by the use of alternative methods of recording the phases of the signals. The admittance curves (Y, Ω^{-1}), may also be used to derive the experimental dispersion relation, since the addition, or subtraction, of one cyclotron half wavelength corresponds to the change from a subsidiary admittance maximum to a minimum. The number of wavelengths between the antennae, for a given antenna spacing, may be found by noting that this is zero at the gyroharmonics, or at ω_T, since the wavelength is then infinite ($k = 0$). This technique has the disadvantages that when ω_H is swept, the electron density may change and d must be large compared with the sheath size. Both methods enable N and T to be measured. In practice it would appear that the use of a swept frequency and tracking receiver to locate ω_T and hence ω_p, together with a measurement of k using the swept (interference) technique would provide a rapid measurement of N and T to a high degree of accuracy. Work is in progress to incorporate a swept frequency transmitter-receiver admittance technique for these purposes. The use of a frequency modulated system to excite a range of wavenumbers may also be useful. Clearly the relatively short wavelengths characteristic of the Bernstein modes make them extremely useful for plasma diagnostic purposes.

Turning now to the work described in the latter part of the paper and concerned with waves near the plasma frequency – it is clear that plasma wave ionograms could provide a useful diagnostic technique particularly for space plasma measurements and that in principle N, ∇N and T may be determined accurately either by computer techniques as described by Thomas, Fang & Andrews (1971) or by an analytic technique (Buckley 1974). The latter requires the detection of the forward and backward waves separately rather than just the beat frequency. In principle this involves the use of a frequency-stable transmitter and a tracking receiver also of high stability in frequency. Single sideband modulation techniques and narrow bandwidth techniques are possible ways of achieving the sensitivity and stability required. The frequency ranges and bandwidths involved for various space and laboratory plasmas requirements have been discussed by Phelps (1971).

The work described in the paper was supported by grants from the Science Research Council. It is a pleasure to acknowledge the contributions made to this work by Dr M. K. Andrews, Dr T. A. Hall and Dr A. D. R. Phelps on the experimental side and by Dr M. T. C. Fang and Dr R. Buckley on ray tracing in hot magnetoplasmas.

PHILOSOPHICAL TRANSACTIONS OF THE ROYAL SOCIETY A MATHEMATICAL, PHYSICAL & ENGINEERING SCIENCES

Appendix A. Theory of plasma wave propagation

In this section, the basic theory of plasma wave propagation in infinite plasma is outlined briefly. Essentially, the problem concerns the application of particle dynamics, through the equations of motion, with Maxwell's equations for the plasma. The latter are written as

$$\nabla\cdot\boldsymbol{D}=\rho,\quad \nabla\cdot\boldsymbol{B}=0,\quad \nabla\times\boldsymbol{E}=-\dot{\boldsymbol{B}},\quad \nabla\times\boldsymbol{H}=\boldsymbol{J}+\dot{\boldsymbol{D}} \tag{A 1}$$

in which $\boldsymbol{E}$, $\boldsymbol{D}$, $\boldsymbol{B}$ and $\boldsymbol{H}$ are the field quantities, $\boldsymbol{J}$ is the current density, ρ, the volume charge density and all quantities are functions of the space variable r and time t. The magnetic induction, $\boldsymbol{B}$, and the field, $\boldsymbol{H}$, are related by $\boldsymbol{B}=\mu_0\boldsymbol{H}$ and the displacement, $\boldsymbol{D}$, and electric field, $\boldsymbol{E}$, are related by $\boldsymbol{D}=\epsilon_0\boldsymbol{E}$ where μ_0 and ϵ_0 are the permeability and permittivity of free space. In analysing plasma behaviour, two approaches are possible. The plasma can be regarded as a region of free space with permittivity ϵ_0 plus an internal assembly of free charges and currents which we shall call ρ_{int} and $\boldsymbol{j}_{\text{int}}$. If a driven antenna is immersed in the plasma, there will be, in addition, a plasma current, $\boldsymbol{j}_{\text{ext}}$, due to the external source charges ρ_{ext}. The first and last Maxwell equations above then become

$$\left.\begin{aligned}\nabla\cdot\boldsymbol{D}&=\nabla\cdot\epsilon_0\boldsymbol{E}=\rho_{\text{int}}+\rho_{\text{ext}}\\ \text{and}\quad \nabla\times\boldsymbol{H}&=\boldsymbol{j}_{\text{ext}}+\boldsymbol{j}_{\text{int}}+\epsilon_0\dot{\boldsymbol{E}}.\end{aligned}\right\} \tag{A 2}$$

Alternatively, we may treat the plasma as a dielectric with a tensor permittivity $\boldsymbol{\varepsilon}(\boldsymbol{k},\omega)$ dependent on the wavenumber $\boldsymbol{k}$ and angular frequency, ω, then equations (A 2) become

$$\left.\begin{aligned}\nabla\cdot\boldsymbol{D}&=\nabla\cdot(\boldsymbol{\varepsilon}\cdot\boldsymbol{E})=\rho_{\text{ext}}\\ \text{and}\quad \nabla\times\boldsymbol{H}&=\boldsymbol{j}_{\text{ext}}+\boldsymbol{\varepsilon}\cdot\dot{\boldsymbol{E}}.\end{aligned}\right\} \tag{A 3}$$

The particle motions must first be expressed in terms of the field quantities $\boldsymbol{E}$, $\boldsymbol{D}$, $\boldsymbol{B}$, $\boldsymbol{H}$ in order to obtain the current density $\boldsymbol{J}$ and the volume charge density ρ. Thus the particle equations of motion have to be considered and these are generally non-linear. As an approximation they are linearized and then transform methods can be used to handle Maxwell's equations and the Boltzmann equation. The method is valid only for small signals.

As stated, the quantities appearing in Maxwell's equations are functions of $\boldsymbol{r}$ and t. They may be transformed into functions of $(\boldsymbol{r},\omega)$ and into functions of $(\boldsymbol{k},\omega)$ by means of the time and space Fourier transforms (A 4) and (A 5) below

$$\boldsymbol{E}(\omega)=\int_{-\infty}^{\infty}\boldsymbol{E}(t)\,\mathrm{e}^{-\mathrm{i}\omega t}\,\mathrm{d}t;\qquad \boldsymbol{E}(t)=\frac{1}{2\pi}\int_{-\infty}^{\infty}\boldsymbol{E}(\omega)\,\mathrm{e}^{\mathrm{i}\omega t}\,\mathrm{d}\omega, \tag{A 4}$$

$$\boldsymbol{E}(\boldsymbol{k})=\int_{-\infty}^{\infty}\boldsymbol{E}(\boldsymbol{r})\,\mathrm{e}^{\mathrm{i}\boldsymbol{k}\cdot\boldsymbol{r}}\,\mathrm{d}\boldsymbol{k};\quad \boldsymbol{E}(\boldsymbol{r})=\frac{1}{(2\pi)^3}\int_{-\infty}^{\infty}\boldsymbol{E}(\boldsymbol{k})\,\mathrm{e}^{-\mathrm{i}\boldsymbol{k}\cdot\boldsymbol{r}}\,\mathrm{d}\boldsymbol{r}. \tag{A 5}$$

In practice we wish to deal with infinite superimposed plane waves (after initial conditions are neglected) in which the quantities involved vary as $\mathrm{e}^{\mathrm{i}(\omega t-\boldsymbol{k}\cdot\boldsymbol{r})}$. This implies infinite plasmas in space. $\boldsymbol{E}(\boldsymbol{r},t)$ may be Laplace transformed in time and further Fourier transformed in space by writing

$$\boldsymbol{E}(\boldsymbol{k},\omega)=\int_{-\infty}^{+\infty}\mathrm{d}\boldsymbol{r}\int_{0}^{\infty}\mathrm{d}t\,\boldsymbol{E}(\boldsymbol{r},t)\,\mathrm{e}^{-\mathrm{i}(\omega t-\boldsymbol{k}\cdot\boldsymbol{r})}. \tag{A 6}$$

The reverse transform is

$$\boldsymbol{E}(\boldsymbol{r},t)=\left(\frac{1}{2\pi}\right)^4\int_{-\infty}^{+\infty}\mathrm{d}\boldsymbol{k}\int_{C}\mathrm{d}\omega\,\boldsymbol{E}(\boldsymbol{k},\omega)\,\mathrm{e}^{\mathrm{i}(\omega t-\boldsymbol{k}\cdot\boldsymbol{r})}. \tag{A 7}$$

It is important to notice that equation (A 6) implies that ω has a negative imaginary part so that the integrand is bounded, which requires the inverse transform (A 7) to be taken along a contour below the real ω-axis.

Maxwell's equations may now be transformed by using $\nabla = -\mathrm{i}\boldsymbol{k}$ and $\partial/\partial t = \mathrm{i}\omega$ and combined to give the wave equation

$$\boldsymbol{k} \times (\boldsymbol{k} \times \boldsymbol{E}) + \omega^2 \mu_0 \boldsymbol{\varepsilon} \cdot \boldsymbol{E} = \mathrm{i}\omega\mu_0 \boldsymbol{j}_{\mathrm{ext}}. \tag{A 8}$$

This includes the effect of the external source (the r.f. driven antenna) and applies only after initial transients have passed. In this equation all the variables represent the doubly transformed quantities. The continuity equation for external charges and currents gives

$$\omega\rho_{\mathrm{ext}} = \boldsymbol{k} \cdot \boldsymbol{j}_{\mathrm{ext}}. \tag{A 9}$$

If we assume $\boldsymbol{k} \times \boldsymbol{E} = 0$ then

$$\omega \boldsymbol{\varepsilon} \cdot \boldsymbol{E} = \mathrm{i}\boldsymbol{j}_{\mathrm{ext}}, \tag{A 10}$$

so that (A 8) reduces to

$$\boldsymbol{E}(\boldsymbol{k}, \omega) = \frac{\mathrm{i}\boldsymbol{k}\rho_{\mathrm{ext}}}{\boldsymbol{k} \cdot \boldsymbol{\varepsilon}(\boldsymbol{k}, \omega) \cdot \boldsymbol{k}}. \tag{A 11}$$

It is important to note that the assumption $\boldsymbol{k} \times \boldsymbol{E} = 0$ implies making the assumption (as in electrostatics) that the electric field (of the wave) is derivable from a potential, ϕ, i.e.

$$\boldsymbol{E} = -\nabla\phi = \mathrm{i}\boldsymbol{k}\phi.$$

Then $\nabla \times \boldsymbol{E} = 0$ and the waves are longitudinal ($\boldsymbol{k} \| E$). From the third Maxwell equation (A 1) it follows that $\boldsymbol{B}$ is also zero so that there is no associated magnetic field for the wave. Thus the potential ϕ is given by

$$\phi = \frac{\rho_{\mathrm{ext}}}{\boldsymbol{k} \cdot \boldsymbol{\varepsilon}(\boldsymbol{k}, \omega) \cdot \boldsymbol{k}}. \tag{A 12}$$

The dispersion equation gives the relation between ω and $\boldsymbol{k}$ for the plasma modes and is obtained by examining (A 11) for non-zero values of $\boldsymbol{E}$ when there is no external source so that $\rho_{\mathrm{ext}} = 0$ and the wave equation is simply $\boldsymbol{k} \cdot \boldsymbol{\varepsilon} \cdot \boldsymbol{k} = 0$.

The wave equation, already simplified by assuming $\boldsymbol{k} \times \boldsymbol{E} \simeq 0$ (i.e. longitudinal modes) is made even more tractable by choosing an appropriate orientation of the coordinate axes with respect to the magnetic field. Thus for propagation perpendicular to $\boldsymbol{B}_0$ (Stix 1962) the dispersion relation is simply

$$k_\perp^2 \epsilon_\perp = 0 \quad \text{or} \quad \epsilon_\perp(\boldsymbol{k}, \omega) = 0, \tag{A 13}$$

and the electric field perpendicular to $\boldsymbol{B}_0$ from (A 11) is

$$\boldsymbol{E}(\boldsymbol{k}, \omega) = \frac{\mathrm{i}\boldsymbol{k}\rho_{\mathrm{ext}}}{k^2 \epsilon_\perp(\boldsymbol{k}, \omega)}. \tag{A 14}$$

Electron oscillations in a warm plasma

When the condition of zero plasma temperature is relaxed, it is necessary for the equations of motion to include thermal motions of the particles and wave-particle interactions through the introduction of the function $f(\boldsymbol{r}, \boldsymbol{v}, t)$ to describe the particle distribution in the plasma. A wave propagating in the plasma sets up electric fields and currents on a microscopic scale which react back on the particle distribution function and thus modify the wave fields. Boltzmann's equation is used to link the fields, currents and the distribution function. This states that the changes in f along a trajectory in phase space are caused only by collisions. If the collision frequency is

sufficiently low, Liouville's equation, which requires that particles are conserved along a trajectory in phase space, may be applied. If the ions are considered to be at rest then for the electron gas

$$\frac{\partial f}{\partial t}+\boldsymbol{v}\cdot\frac{\partial f}{\partial \boldsymbol{r}}-\frac{e}{m}(\boldsymbol{E}+\boldsymbol{v}\times\boldsymbol{B})\cdot\frac{\mathrm{d}f}{\mathrm{d}\boldsymbol{v}}=0, \tag{A 15}$$

where $\boldsymbol{r}$, $\boldsymbol{v}$ and m are the electron position vector, velocity and mass respectively and this equation links the distribution function with the fields in the plasma. It is then assumed that any wave-like disturbance propagates through the medium as $\exp \mathrm{i}(\omega t-\boldsymbol{k}\cdot\boldsymbol{r})$ where $\boldsymbol{k}$ is the wavenumber and ω is the (complex) angular frequency, i.e. f is expressed as a steady component f_0 plus a small perturbation $f_1 \propto \exp \mathrm{i}(\omega t-\boldsymbol{k}\cdot\boldsymbol{r})$. Equation (A 15) is then written to include only first order terms as a linearized equation. For an account of how this equation was then solved, and the assumptions involved, the reader is referred to the paper by Thomas & Andrews (1969) in which a presentation is given based on the treatment of Bernstein (1958) who first correctly solved it explicitly. Equation (4.7) in the paper by Thomas & Andrews (1969) gives the general dispersion relation relating ω and $\boldsymbol{k}$ for small amplitude waves in any electron gas described by a distribution function $f_0(\boldsymbol{r}, \boldsymbol{v}, t)$ based on the derivation of Bernstein (1958) and the 'electrostatic' assumption discussed earlier. If the function, f_0, corresponds to a Maxwellian velocity distribution for the electrons in the plasma then the equation may be integrated progressively to yield

$$1+k^2a^2=\frac{s}{\omega_H}\int_0^\infty \mathrm{d}y \exp\left[-\frac{sy}{\omega_H}-\Lambda_s(1-\cos y)-\tfrac{1}{2}\Lambda_c y^2\right], \tag{A 16}$$

where a is the Debye length (see table 2), $s=\mathrm{i}\omega$, the Laplace transformed frequency, $\Lambda_s=k^2r^2\sin^2\theta$ (r is defined in table 2), $\Lambda_c=k^2r^2\cos^2\theta$, θ is the angle between $\boldsymbol{k}$ and the field $\boldsymbol{B}_0$, and y is the variable of integration $\phi'-\phi$ (Thomas & Andrews 1969).

This integral is defined for all s if $\Lambda_c > 0$, or if s has a small real component. The electron oscillations parallel to the applied magnetic field are given by (A 16) with $\Lambda_s = 0$, while the cyclotron modes emerge when the propagation is at right angles to $\boldsymbol{B}_0$, i.e. $\Lambda_c = 0$. For this propagation mode, Bernstein (1958) showed that the damping caused by wave-particle interactions is zero, that is, ω is real and s is imaginary. As the direction of propagation is varied from the perpendicular, Landau damping increases extremely rapidly, and is rather wavelength dependent. Near 90° the damping depends strongly on whether ω is near a multiple of the electron gyrofrequency. (A 16) with $\Lambda_c = 0$ when integrated yields

$$k^2a^2=\mathrm{e}^{-\Lambda}I_0(\Lambda)+2\sum_{n=1}^{n=\infty}\mathrm{e}^{-\Lambda}I_n(\Lambda)\frac{\Omega^2}{\Omega^2-n^2}-1, \tag{A 17}$$

where I_n is a Bessel function of the first kind, of imaginary argument (see also table 2). Clearly from the first of (A 13) and the dispersion relation (A 17), it follows that $\epsilon_\perp(k,\omega)$ is given by equation (3) quoted earlier. Clearly poles will be produced each time Ω approaches an integer and the solutions of (A 17) are given by the intersection of a horizontal line of ordinate k^2a^2 with the Bessel series $\alpha(\Omega,\lambda)$ given by the right hand side of (A 17). For reasonably large values of k^2a^2 there are then an infinite number of solutions of Ω all close to, but slightly greater than, integers.

Integral representations of (A 17) are also available and these, together with a discussion of numerical solutions of (A 17) obtained both by the series and integral solutions are given in Andrews (1969), and in Thomas & Andrews (1969). Numerical solutions were earlier obtained by Crawford *et al.* (1967).

The range of wavelengths (or of $k_\perp r$) is not unlimited. Though in theory the wavelength could become infinitely short, in practice wavelengths less than the Debye length are excluded on physical grounds since the waves would not then be subject to collective particle effects and the wave fields would be influenced by individual particle trajectories. Thus $2\pi/k > a$, i.e. $k_\perp r < 2\pi\omega_p/\omega_H$. At the long wavelength end, the condition $\omega/k \ll c$ (implied by the 'electrostatic' assumption) becomes $\Omega/kr < c/v_T$ where v_T is the thermal velocity of an electron. For $c/v_T \approx 1000$, computed solutions become invalid above the light line $\Omega = 1000k_\perp r$ and the curves do not approach the $k_\perp r = 0$ axis with zero slope in the wedge-shaped zone where electromagnetic effects must be taken into account.

Effect of collisions

At distances greater than a few Debye lengths from an antenna immersed in a plasma, linear theory, as described later, may be applied. The theory can be made more realistic by the inclusion of a term to represent collisions in the Boltzmann equation which then becomes formally equivalent to the collisionless Liouville equation (A 15) if ω is replaced by $\omega - i\nu$ where ν is the electron-neutral collision frequency in a lightly ionized plasma. For an infinite plane grid at $x = 0$ in the (yz) plane, parallel to $\boldsymbol{B}_0$, driven by an oscillating charge ρ_{ext} at a frequency ω_0, we have, writing δ for the Dirac delta-function

$$\rho_{ext} = \rho_0 e^{i\omega_0 t}\,\delta(x). \tag{A 18}$$

The double transform gives for $\rho_0 = 1$,

$$\rho_{ext}(k, \omega) = \frac{1}{i(\omega - \omega_0)}. \tag{A 19}$$

(A 14) and (A 7) may be used to give the temporal electric field perpendicular to the grid

$$\boldsymbol{E}(k, t) = \boldsymbol{k}\frac{1}{2\pi k^2}\int_C \frac{e^{i\omega t}\,d\omega}{\epsilon_\perp(\omega - i\nu, k)\,(\omega - \omega_0)}. \tag{A 20}$$

For real k, the roots ω of $\epsilon_\perp(k, \omega) = 0$ are real, thus the zeros of $\epsilon_\perp(k, \omega - i\nu)$ now lie at $\omega + i\nu$. For large t, the electric field arising from a real wavenumber is

$$\boldsymbol{E}(k, t) = i\boldsymbol{k}\frac{e^{i\omega_0 t}}{k^2\epsilon_\perp(k, \omega_0 - i\nu)}, \tag{A 21}$$

and the system responds only to the driving frequency ω_0 and all time dependences are of the form $e^{i\omega_0 t}$. The spatial electric field $E(x, t)$ is then given by (5). The value of k required to reduce $\epsilon_\perp$ to zero may be determined and is such that the root (ω_0, k_0) moves to $(\omega_0 - i\nu, k_0 - i\nu/v_g)$ where v_g is the group velocity and the poles no longer fall on the integration path in (5). For $x > 0$, only the shifted poles corresponding to $-k_1$ and $+k_2$ in figure 1, i.e. the portions of the dispersion curve with positive group velocities contribute to the field. Thus, even though one mode has a negative phase velocity, energy is carried away from the antenna as physically expected.

Appendix B: Antennae in a plasma (theory)

Parallel infinite grids immersed in a plasma

The case of two parallel conducting infinite grids has been considered by Mantei (1967) and by Buckley (1968, 1970). Mantei (1967) assumes a charge density of $\pm\rho_0$ coulombs per unit area so that the magnitude of the total current satisfies

$$I_0 = \dot{\rho}_{ext} = i\omega\rho_0 e^{i\omega t},$$

and $$\rho_{\text{ext}}(x, \omega) = \rho_0 e^{i\omega t}[\delta(x - x_0) - \delta(x + x_0)],$$

in which δ is the Dirac delta-function. Transforming and substituting for ρ_{ext} into the wave equation (2) for $E(k, \omega)$ and applying the inverse transformation to give the $E(x, \omega)$ field perpendicular to $\boldsymbol{B}_0$ yields

$$E(x, \omega) = \frac{\rho_0}{\pi} e^{i\omega t} \int_{-\infty}^{+\infty} \frac{\sin(k_\perp x_0)\, e^{-ik_\perp x}\, dk_\perp}{k_\perp \epsilon(k_\perp, \omega)}, \tag{B 1}$$

where $2x_0$ is the distance between the grids. Note that when ω is within the Bernstein mode pass bands, purely real roots of $\epsilon_\perp$ lie on the real $k_\perp$ axis. However, the integrand above is not defined on the real $k_\perp$ axis. The $k_\perp$ integration may be performed, however, by deforming the path of integration round the real roots. The field is then regarded as made up of two parts – the principal value evaluated over the real $k_\perp$ axis (and corresponding to the capacitively coupled field since there is no dependence on $k_\perp$) plus the residues of the integrand evaluated at the singularities k_1 and k_2 which correspond to the propagating Bernstein modes. Integrating the electric field over x gives the voltage between the grids so that the impedance, Z per unit area is obtained by dividing by the current I_0. The admittance per unit area (corresponding to the current supplied from the external source to keep the voltage between them at a constant value) is given by $1/Z$ as

$$Y(\omega) = i\pi\omega \Big/ 2 \int_{-\infty}^{\infty} \frac{\sin^2(k_\perp x_0)\, dk_\perp}{k_\perp^2 \epsilon(k_\perp, \omega)}. \tag{B 2}$$

One can see immediately from this that the admittance will contain an oscillatory component arising from the $\sin^2$ terms as well as a contribution arising from the behaviour of the denominator of the integrand. To carry out the integration Mantei (1967) introduced a non-zero collision frequency into the expression for $\boldsymbol{E}$ (see (5)). The roots of $\epsilon(k_\perp, \omega)$ then become complex and the integration can be performed entirely along the real $k_\perp$ axis. The results of numerical computations by Mantei (1967) show that

(1) The conductance is relatively large within the pass-bands and exhibits oscillations with maxima corresponding to the minima in $\sin k_\perp x$ in (B 2). The susceptance also shows the oscillations.

(2) Both components of the admittance minimize at ω_T and at the high frequency end of the pass bands above ω_T.

(3) The behaviour of the roots of $\epsilon(k_\perp, \omega)$ in the complex $k_\perp$ plane is such that both components of the admittance have peaks at the gyroharmonics $\omega = n\omega_H$ for $n \geqslant 2$. For $n = 1$ the susceptance also maximizes but the conductance does not since $k \to \infty$ and collisional damping is very high. For $n \geqslant 2$, G maximizes when the frequency approaches $\omega = n\omega_H$ from above, i.e. from within the pass-band. S maximizes when the harmonic is approached from below. The roots merge towards the integration contour as ω passes through a cyclotron harmonic from above, within the pass band, and then separate out again, the admittance maximizing at the frequency of closest approach to the integration contour, i.e. closest to the cyclotron harmonic.

Buckley (1968, 1970) in an analysis similar to that of Mantei (1967) has expressed the electric field $E(x, t)$ corresponding to the integral expression (B 1) in the series form already given as equation (9).

Parallel wire admittance

The experiments described in the text were performed using thin antennae made of wire rather than grids. The thin wire antennae may be assumed to correspond to two infinitely long parallel line charges in a direction parallel to $\boldsymbol{B}_0$ or two thin parallel cylindrical conductors provided the potential field due to one cylinder is not distorted by the presence of the other. In a similar analysis to that described for grids, Mantei (1967) derives an expression (22) for the normalized plasma impedance. Noting that the vacuum impedance between two conducting cylinders radius a, distance $2x_0$ apart is given by

$$Z = \frac{1}{\mathrm{i}\omega C_0} \simeq \frac{\ln(2x_0/a)}{\mathrm{i}\omega\pi\epsilon_0},$$

(22) can be inverted to give the admittance

$$Y(\omega) = \mathrm{i}\omega\pi \Big/ \int_0^\infty \frac{J_0(k_\perp a) - J_0(2k_\perp x_0)\,\mathrm{d}k_\perp}{k_\perp \epsilon(k_\perp, \omega)}. \tag{B 3}$$

Numerical solutions of an equation corresponding to (B 3), but, including a collision frequency term, show that the admittance components behave qualitatively in precisely the same way as in the parallel grid case already described in some detail.

References (Thomas)

Andrews, M. K. 1969 Plasma studies related to observations made by ionospheric top-side sounder satellites, Ph.D. Thesis, Imperial College, University of London.

Andrews, M. K. & Fang, M. T. C. 1971 *J. Plasma Phys.* (3) **6**, 579–587.

Bernstein, I. B. 1958 *Phys. Rev.* **109**, 10–21.

Buckley, R. 1968 R.F. Characteristics of a plane-grid capacitor immersed in a hot collision-free plasma with uniform magnetic field parallel to the grid plates: Radio and Space Research Station Report, Slough, U.K.

Buckley, R. 1970 *Plasma waves in space and laboratory* (ed. J. O. Thomas & B. J. Landmark), vol. 2, 129–158. Edinburgh: University Press.

Buckley, R. 1974 The topside sounder resonance at the plasma frequency, Report No. SP-T01-74: Imperial College, University of London.

Clinckemaillie, A. 1970 *Plasma waves in space and laboratory* (ed. J. O. Thomas & B. J. Landmark), vol. 2, 243–270. Edinburgh: University Press.

Cook, I. 1974 *Plasma physics* (ed. B. E. Keen). Conference Series No. 20, 225–241. London: The Institute of Physics.

Crawford, F. W. 1969 *Plasma waves in space and laboratory* (ed. J. O. Thomas & B. J. Landmark), vol. 1, 125–156. Edinburgh: University Press.

Crawford, F. W., Harp, R. S. & Mantei, T. D. 1967 *J. geophys. Res.* **72**, 57–68.

Crawford, F. W., Kino, G. S. & Weiss, H. H. 1964 *Phys. Rev. Lett.* **13**, 229–232.

Derfler, H. 1974 Excitation of plasma waves by gaps and slow-wave structures, IPP IV/77, Report: Max-Planck-Institut fur Plasmaphysik, Garching-bei Munchen.

Dougherty, J. P. 1974 *Plasma physics* (ed. B. E. Keen). Conference Series No. 20, 21–54. London: The Institute of Physics.

Dreicer, H. 1969 *Plasma waves in space and laboratory* (ed. J. O. Thomas & B. J. Landmark), vol. 1, 157–194. Edinburgh: University Press.

Fang, M. T. C. 1971 Ray-tracing in hot magnetoplasma. Report No. SP-T102–71; Imperial College, University of London.

Fang, M. T. C. & Andrews, M. K. 1971 *J. Plasma Phys.* (3) **6**, 567–577.

Fejer, J. A. & Yu, W.-M. 1970 *J. Geophys. Res.* (10) **75**, 1919–1925.

Franklin, R. N. 1974 *Plasma physics* (ed. B. E. Keen). Conference Series No. 20, 197–224. London: The Institute of Physics.

Fredricks, R. W. 1968 *J. Plasma Phys.* **2**, 365–380.

Graff, P. 1971 *J. Plasma Phys.* **5**, 427–439.

Hall, T. A. & Landauer, G. 1971 *Radio Sci.* (11) **6**, 967–980.

PHILOSOPHICAL TRANSACTIONS OF THE ROYAL SOCIETY A MATHEMATICAL, PHYSICAL & ENGINEERING SCIENCES

Harp, R. S. 1965 *Appl. Phys. Lett.* **6**, 51–53.
Keen, B. E. (ed.) 1974 *Plasma physics*. Conference Series No. 20. London: The Institute of Physics.
Knecht, R. W., van Zandt, T. E. & Russell, S. 1961 *J. Geophys. Res.* **66**, 3078–3081.
Landau, L. D. 1946 *J. Phys. U.S.S.R.* **10**, 25–34.
Leuterer, F. 1969 *Plasma Phys.* **11**, 615–620.
Lockwood, G. E. K. 1963 *Canad. J. Phys.* **41**, 190–194.
Mantei, T. D. 1967 *Cyclotron harmonic wave phenomena*, Institute for Plasma Physics Report No. 194: Stanford University.
McAfee, J. R. 1968 *J. Geophys. Res.* **73**, 5577–5583.
McAfee, J. R. 1969*a* *J. Geophys. Res.* **74**, 802–808.
McAfee, J. R. 1969*b* *J. Geophys. Res.* **74**, 6403–6408.
Parkes, E. J. 1974*a* *J. Plasma Phys.* (2) **12**, 199–216.
Parkes, E. J. 1974*b* *J. Plasma Phys.* (2) **12**, 217–232.
Phelps, A. D. R. 1971 Report No. SP-T101–71: Imperial College, University of London.
Sanderson, J. J. 1974 *Plasma phyics* (ed. B. E. Keen). Conference Series No. 20, 55–92. London: The Institute of Physics.
Stix, T. H. 1962 *The theory of plasma waves*. New York: McGraw-Hill.
Thomas, J. O. & Andrews, M. K. 1969 *Plasma waves in space and laboratory*, (ed. J. O. Thomas & B. J. Landmark), vol. 1, 3–39. Edinburgh: University Press.
Thomas, J. O., Andrews, M. K. & Hall, T. A. 1970 *Experimentally measured dispersion properties of plasma cyclotron waves*, Report No. SP-T105-70: Imperial College, University of London.
Thomas, J. O., Andrews, M. K., Hall, T. A. & Phelps, A. D. R. 1971 *Proc. 10th Int. Conf. on Phenomena in Ionized Gases* 1971, (ed. R. N. Franklin), University of Oxford, p. 314. Oxford: Donald Parsons & Co. Ltd.
Thomas, J. O., Fang, M. T. C. & Andrews, M. K. 1971 *Proc. 10th Int. Conf. on Phenomena in Ionized Gases* 1971, (ed. R. N. Franklin), University of Oxford, p. 428. Oxford: Donald Parsons & Co. Ltd.
Thomas, J. O. & Landmark, B. J. (eds) 1969 *Plasma waves in space and laboratory*, vol. 1. Edinburgh: University Press.
Thomas, J. O. & Landmark, B. J. (eds) 1970 *Plasma waves in space and laboratory*, vol. 2. Edinburgh: University Press.
Wesson, J. A. 1974 *Plasma physics* (ed. B. E. Keen). Conference Series No. 20, 93–130, London: The Institute of Physics.

PHILOSOPHICAL TRANSACTIONS OF THE ROYAL SOCIETY A MATHEMATICAL, PHYSICAL & ENGINEERING SCIENCES

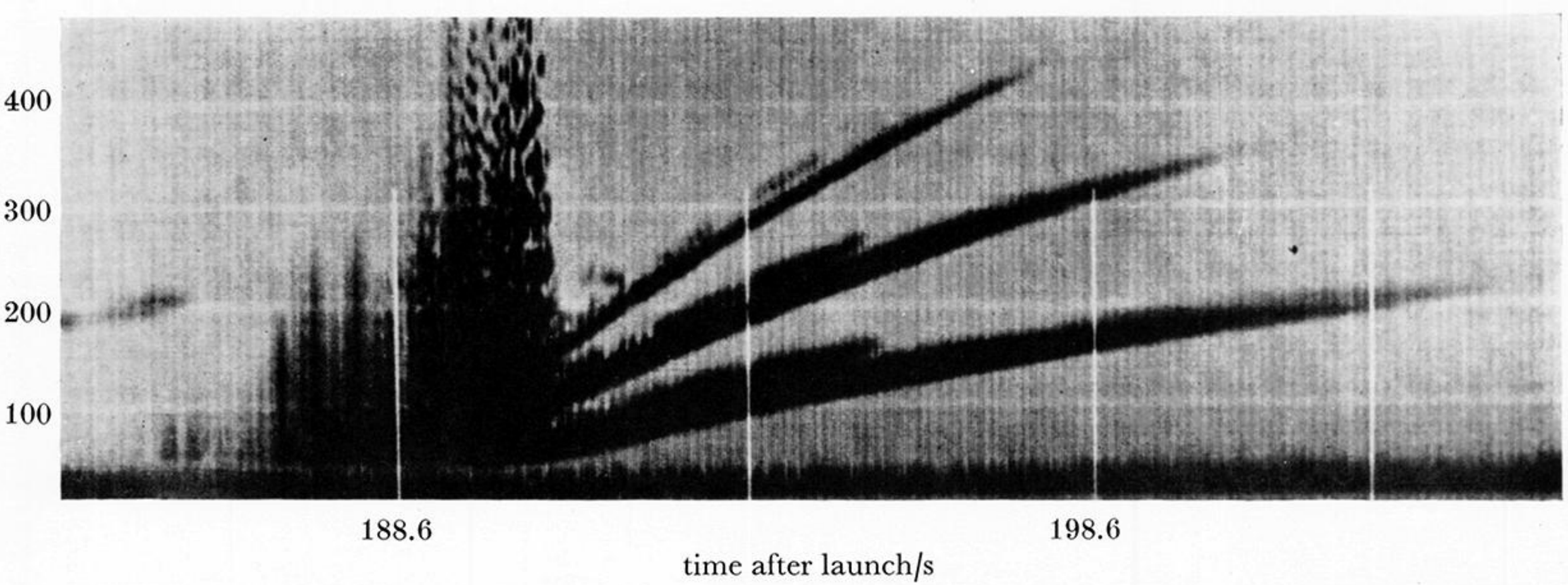

FIGURE 11. Early observations of a 'plasma resonance spike' excited by a rocket-borne transmitter immersed in the ionospheric plasma. The time delay, or vertical depth of reflexion, of signals near a frequency of 5.97 MHz is recorded as a function of flight time (after Knecht *et al.* 1961). Record made 24 June 1961, 18h17 LMT.

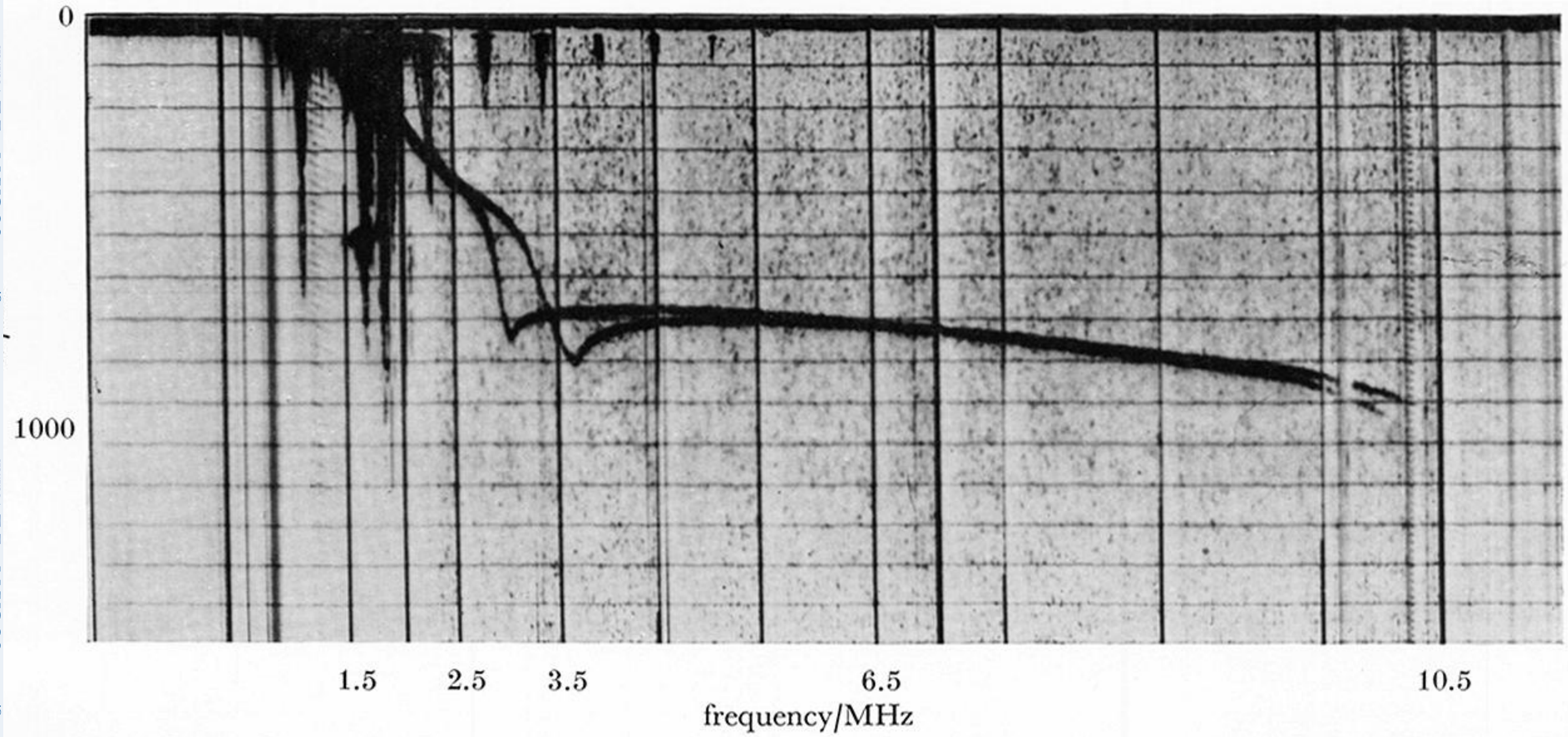

FIGURE 13. An actual Alouette I topside ionogram recorded at low latitudes. The ordinate is the virtual depth of reflexion of the signal. The vertical lines are frequency markers. Both the electro-magnetic wave returns and plasma wave returns are clearly visible (cf. figure 12).

PHILOSOPHICAL TRANSACTIONS OF THE ROYAL SOCIETY A MATHEMATICAL, PHYSICAL & ENGINEERING SCIENCES

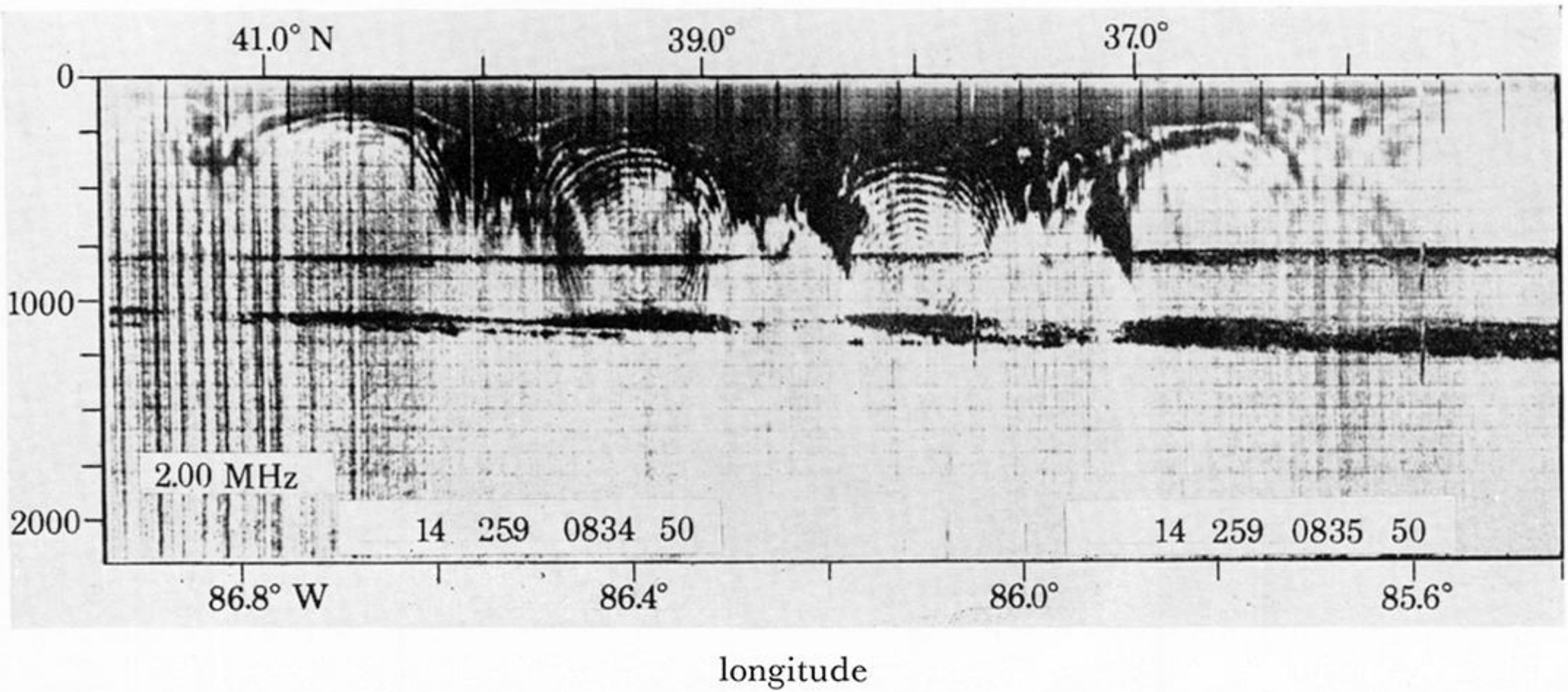

FIGURE 15. Part of a film record from the Explorer XX satellite in which the virtual depth of reflection of a transmitted pulse (here 2 MHz) is recorded as a function of time. The 'resonance' or plasma wave signals appear as a continuous echo modulated in virtual depth by the roll motion of the satellite antennae. The interference pattern arises from the beating of two plasma waves of different wavelengths. (15 Sept. 1964/0834Z/0248 LMT, $f_H = 1.02$ MHz, satellite height = 968 km).